A cytomegalovirus immunevasin triggers integrated stress response-dependent reorganization of the endoplasmic reticulum.

Running Title: HCMV UL148 reorganizes the ER.

Hongbo Zhang[a,1], Clarissa Read[d,e,1], Christopher C. Nguyen[a,1], Mohammed N.A. Siddiquey[a], Chaowei Shang[c], Cameron M. Hall[a], Jens von Einem[d], and Jeremy P. Kamil[a,b #]

[a]Department of Microbiology and Immunology,

[b]Center for Molecular and Tumor Virology

[c]Research Core Facility

LSU Health Sciences Center, Shreveport, Louisiana, USA

[d] Institute of Virology, Ulm University Medical Center,

[e]Central Facility for Electron Microscopy, Ulm University

Ulm, Germany

[1] these authors contributed equally to the study

Running Head: HCMV UL148 Remodels the ER

#Address correspondence to Jeremy P. Kamil, jkamil@lsuhsc.edu

ABSTRACT. Human cytomegalovirus (HCMV) encodes an ER-resident glycoprotein, UL148, which activates the unfolded protein response (UPR) but is fully dispensable for viral replication in cultured cells. Hence, previously ascribed roles of UL148 in immune evasion and modulation of HCMV cell tropism are hypothesized to cause ER stress. Here, we show that UL148 is necessary and sufficient to drive the formation of large ER-derived structures that occupy up to 7% of the infected cell cytosol, and which represent sites where UL148 coalesces together with ER quality control proteins such as the E3 ubiquitin ligase Hrd1 and the ER mannosidase EDEM1. Ultrastructural analyses of the structures reveal tortuous, densely packed segments of collapsed ER which connect to distended cisternae. Notably, we observe that UL148 accumulates in a detergent-insoluble form during infection while a homologous rhesus cytomegalovirus immunevasin that fails to cause ER reorganization remains soluble. During induced ectopic expression of UL148-GFP fusion protein, punctate signals are observed that traffic to accumulate at prominent structures that exhibit poor recovery of fluorescence after photobleaching. Small molecule blockade of the integrated stress response (ISR) prevents puncta formation, leading to a uniform reticular fluorescent signal. Accordingly, ISR inhibition during HCMV infection abolishes the coalescence of UL148 and Hrd1 into discrete structures. Given that UL148 stabilizes within the ER the receptor binding subunit of an alternative viral envelope glycoprotein complex that is required for infectivity, our results imply stress-dependent ER remodeling contributes to viral cell tropism.

48 **IMPORTANCE.**

49 Perturbations to ER morphology occur during infection with various intracellular
50 pathogens and in certain genetic disorders. We identify that an HCMV gene product,
51 UL148, profoundly reorganizes the ER during infection, and is sufficient to do so when
52 expressed on its own. Although several viruses reorganize the ER, the viral proteins
53 necessary for such effects often play essential roles in viral replication. Although UL148
54 is fully dispensable for HCMV replication in cultured cells, UL148 intercepts the immune
55 cell co-stimulatory ligand CD58 before it reaches the cell surface and influences the
56 composition of viral envelope glycoprotein complexes required for cell entry. We find
57 that UL148 requires integrated stress response (ISR) to cause ER reorganization. Our
58 results reveal UL148-dependent reorganization of the ER as a prominent feature of
59 HCMV infected cells and provide a basis for the use of UL148 to screen for novel ISR
60 inhibitors.

61 **INTRODUCTION.**

62 UL148 is a human cytomegalovirus (HCMV) ER-resident glycoprotein that plays
63 roles in evasion of cell-mediated immunity and shows intriguing effects on cell tropism.
64 During infection of epithelial cells, viruses disrupted for *UL148* replicate to produce
65 roughly 100-fold enhanced levels of infectious progeny virions compared to wildtype (1).
66 These effects correlate with reduced expression of glycoprotein O (gO), a subunit of a
67 heterotrimeric viral glycoprotein H (gH) / glycoprotein L (gL) complex (gH/gL/gO) on the
68 virion envelope that is required for the infectivity of cell-free virions (2-4), and which
69 endows the virus with the capacity to utilize the platelet derived growth factor receptor α
70 (PDGFRα) as an entry receptor (5-7). Accordingly, UL148 has been found to stabilize
71 immature forms of gO prior their assembly into gH/gL/gO heterotrimers (1, 8). Despite
72 that UL148 does not stably associate with gO, the data suggest that it may interact with
73 gH (1).

74 UL148 also physically associates with CD58 (LFA-3), a co-stimulatory ligand for
75 natural killer cells and T-lymphocytes, preventing its presentation at cell surface (9).
76 Although the mechanisms by which UL148 stabilizes gO and retains CD58 within the
77 ER remain unknown, UL148 strongly contributes to activation of the unfolded protein
78 response (UPR) during infection, and is sufficient to activate the UPR when ectopically
79 expressed in non-infected cells (10). UL148 co-purifies from infected cells with SEL1L,
80 an adaptor subunit of ER-based E3 ubiquitin ligase Hrd1 that that plays important roles
81 in ER-associated degradation (ERAD) of terminally misfolded glycoproteins (8). Hence,
82 the potential association of UL148 with the ERAD machinery may suggest a mechanism
83 for its activation of the UPR.

84 Here, we show that expression of UL148 is necessary and sufficient to induce
85 unusual ER structures at which large quantities of ER factors involved in glycoprotein
86 quality control accumulate. In electron microscopy analyses, we find that the UL148
87 induced ER-structures are comprised of densely packed, tortuous ER membranes that
88 form connections with tubules of highly distended cisternal space. Our results may
89 have implications for understanding the mechanisms by which UL148 regulates viral cell
90 tropism and contributes to viral evasion of cell-mediated immunity. Further, our findings
91 suggest that ER remodeling events triggered by UL148 are indicative of an adaptive
92 response of eukaryotic cells to proteotoxic stress involving the secretory pathway.
93

94 **RESULTS.**

95

96 **UL148 causes reorganization of ER quality control proteins into unusual globular**
97 **structures.**

98 The HCMV ER-resident glycoprotein UL148 was previously observed to co-
99 localize with the ER marker calnexin during infection (1). Nonetheless, the calnexin
100 staining did not show the uniform reticular staining pattern characteristic for the ER
101 marker. However, we later noticed that cells infected with a *UL148*-null virus but not an
102 isogenic wildtype control showed uniform calnexin staining (see below). To formally
103 determine whether UL148 influences calnexin localization, we compared fibroblasts at
104 four days post-infection with either wildtype (TB_WT) or *UL148*-null mutant
105 (TB_148STOP) viruses derived from HCMV strain TB40/E (**FIG 1**). In cells infected with
106 wildtype virus, calnexin antibodies stained unusual globular structures at the cell
107 periphery, as expected (1) (**FIG 1A, 1C, SI FIG S1A**). However, in cells infected with
108 the *UL148*-null virus, calnexin staining was uniform throughout the cytosol (**FIG 1B-C**),
109 as would be expected for an ER marker in uninfected cells. The staining pattern for
110 Hrd1, another ER marker, likewise indicated accumulation at unusual globular
111 structures during wildtype HCMV infection, but not during infection with *UL148*-null
112 mutant viruses (**FIG 1, SI FIG S1A**). Because calnexin and Hrd1 staining showed
113 uniform distribution in *UL148*-null virus infected cells, and because *UL148* is fully
114 dispensable for efficient viral replication in fibroblasts (1), these results suggest that
115 redistribution of these ER markers during HCMV infection depends on UL148.

116 As expected (11, 12), antibodies specific for the HCMV envelope glycoprotein,
117 glycoprotein H (gH), stained a juxtanuclear compartment discrete from the ER, termed
118 the cytoplasmic virion assembly compartment (cVAC) (**FIG 1**). Localization of gH to the
119 cVAC was readily apparent in both wildtype and *UL148*-null virus infected cells. Similar
120 staining patterns for Hrd1 and/or calnexin were observed in cells infected with wildtype
121 or *UL148*-null mutants of clinical HCMV strains Merlin and TR, and in four primary
122 clinical isolates grown directly from throat swabs of infected patients (**SI, FIG S1B-D**).
123 Furthermore, similar differences in Hrd1 staining were observed between WT and
124 *UL148*-null viruses during infection of THP-1 macrophages and ARPE-19 epithelial cells
125 (**SI, FIG S1E**). Thus, the UL148-dependent effects on localization of calnexin and Hrd1
126 are not an anomaly particular to strain TB40/E. Nor does UL148-dependent
127 redistribution of ER markers occur only during infection of fibroblasts. These results
128 suggest that UL148-dependent redistribution of calnexin and Hrd1 occurs many if not all
129 cell types during wildtype HCMV infection.
130 We measured the three-dimensional volume of UL148-dependent Hrd1
131 structures from sixteen infected cells. We found that on average the structures
132 occupied 303.3 μm^3 (SEM: +/- 24.8) out of a total cell volume of 7657 μm^3 (SEM:+/-
133 651.0), as estimated by using a phalloidin-fluorophore conjugate to visualize the actin
134 cytoskeleton (**FIG 1E**). Subtracting the volume of nuclei, as indicated by 4′,6-diamidino-
135 2-phenylindole [DAPI] (average nucleus: 1360 μm^3, SEM:+/-129.4), we calculate that,
136 on average, the structures occupy 5.2% of the cytosolic volume (SEM: +/-0.61%, range:
137 2.0% – 7.0%). Based on these findings, taken together with results comparing

138 additional WT versus *UL148*-null mutant HCMV strains (**FIG S1**), we conclude that the
139 UL148-dependent ER structures are a prominent feature of HCMV-infected cells.
140 UL148 substantially contributes to activation of the unfolded protein response
141 (UPR) during HCMV infection (10), and co-purifies from infected cells with SEL1L (8),
142 an adaptor subunit for the E3 ubiquitin ligase Hrd1, which plays crucial roles in ER-
143 associated degradation (ERAD) of terminally misfolded glycoprotein substrates (13).
144 Hence, the accumulation of Hrd1 and calnexin at unusual structures during wildtype but
145 not *UL148*-null infection may suggest that the formation of these ER structures occurs in
146 response to defects in ER quality control (ERQC) caused by UL148. Under conditions
147 of proteasome inhibition, overexpression of certain misfolded glycoproteins causes
148 cellular factors involved in ERQC, such as calnexin to compartmentalize from the rest of
149 the ER, while other ER markers such as BiP (Grp78) or protein disulfide isomerase
150 remain largely unaltered (PDI) (14-16).
151 To gain further insights into the nature of these peculiar ER structures, we set out
152 to develop a more comprehensive understanding of their protein composition by
153 comparing the localization of selected ER markers in cells fixed at 96 h post-infection
154 (hpi) either with TB_148^{HA} (1), a derivative of HCMV strain TB40/E that expresses at the
155 C-terminus of UL148 the nonapeptide epitope YPYDVPDYA from influenza A
156 hemagglutinin (HA), or with TB_159^{HA}, an isogenic control virus in which we replaced
157 the *UL148* coding sequence with the UL148 homolog from rhesus cytomegalovirus,
158 Rh159, likewise fused at its C-terminus to an HA-tag. We considered the TB_159^{HA}
159 virus to be an appropriate control for the following reasons. Firstly, Rh159 and UL148
160 exhibit ~30% identity at the amino acid level and both glycoproteins localize to the ER

161 and block cell surface presentation immune cell activating ligands; UL148 retains CD58,
162 a ligand for CD2, while Rh159 retains NKG2D ligands of the MIC- and ULBP families (1,
163 9, 17). Secondly, Rh159 is expressed from TB_159^{HA} at comparable levels and with
164 similar kinetics observed for UL148 from TB_148^{HA}, and the two viruses replicate
165 indistinguishably in fibroblasts (**FIG 2**). Moreover, Rh159 does not appear to activate
166 the UPR (10), and ERQC markers fail to coalesce into unusual structures during
167 infection with TB_159^{HA} (**FIG 3**). Notably, ER structures fail to occur in rhesus
168 fibroblasts during infection with a recombinant rhesus cytomegalovirus (RhCMV)
169 engineered to express an HA-tag fused at the C-terminus of Rh159 (**FIG S1F**). This
170 argues against the possibility that Rh159 might somehow require the context of rhesus
171 cells to redistribute ER markers in a manner analogous to what is seen for UL148
172 during HCMV infection.

173 In cells infected with TB_148^{HA}, HA antibody staining indicated localization of
174 UL148 to globular structures, as expected (1). Antibody signals during indirect confocal
175 immunofluorescence detection of cellular ER resident proteins involved in ERQC,
176 including calnexin, Hrd1, SEL1L, Herp, valosin containing protein (VCP, p97), and
177 EDEM1, co-localized to a strong degree with signals from HA antibody detection of HA-
178 tagged UL148 (**FIG 3-4**). These results indicate that a number of ERQC factors
179 coalesce with UL148 to form prominent globular structures in infected cells. In contrast,
180 uniform ER staining patterns were observed with antibodies specific for PDI and
181 calreticulin (CALR), indicating that these ER markers do not co-localize to the UL148
182 structures (**FIGS 3Q, 3S**). Intriguingly, ER markers for smooth and rough ER,
183 ribophorin 1 and reticulon 3, both co-localized with UL148 (HA) signal at the structures

184 (**FIGS 3K, 3M)**. This result suggests that rough and smooth ER may participate in the
185 ER structures. LC3B failed to co-localize with the structures (**FIG S2**), as expected
186 since macroautophagy is blocked at late times during HCMV infection (18, 19).
187 However, our results indicate that a related ATG8 family protein, GABARAP, co-
188 localizes with UL148 at the induced structures (**FIG 3O**).

189 In cells infected with TB_159^{HA}, all of the ER markers we examined showed
190 uniform, reticular staining, as did the anti-HA signal detecting Rh159 (**FIG 3B, D, F, H,**
191 **J, L, N, P, R, T**). EDEM1, in addition to showing reticular staining, also labeled puncta
192 associated with the nucleus (**FIG 3J**), which may represent enriched levels of the
193 protein at the rough ER membranes associated with the nuclear envelope, although we
194 cannot exclude the possibility of spurious intranuclear staining. Nonetheless, the
195 punctate nuclear signal for EDEM1 was much less pronounced in the TB_148^{HA}
196 infected cells (**FIG 3I**). GABARAP antibodies stained the cVAC in TB_159^{HA} infected
197 cells, but also showed a much weaker reticular signal that may indicate ER staining.
198 Even though we took steps to block viral Fc receptors, which can cause rabbit
199 antibodies to non-specifically label the cVAC (20), it is plausible that GABARAP
200 antibody signal from the cVAC reflects incomplete blocking of viral Fc receptors. For
201 both viruses, antibodies specific for syntaxin-6 (STX6) and gH, as expected, stained the
202 juxtanuclear cVAC structure (11, 12, 21), which was previously found to be altogether
203 distinct from the UL148 staining pattern (1)(**FIG S2**).

204 To quantify the degree of co-localization with UL148, we calculated Pearson's
205 correlation coefficients from a minimum of thirty TB_148^{HA} infected cells per staining
206 condition, comparing the signal overlap for each ER marker to the HA signal from

207 UL148. The correlation coefficients (*r*) for EDEM1, Hrd1, reticulon-3 (RTN3), SEL1L
208 and calnexin ranged from 0.8 to 0.72, which suggests that these proteins strongly co-
209 localize with UL148 by 4 days post-infection (dpi) (**FIG 4**). Meanwhile, GABARAP,
210 VCP, ribophorin-1 (RPN1), and Herp showed *r* values in the range of 0.54 to 0.51,
211 indicating moderate co-localization with UL148. As expected, the ER markers CALR
212 and PDI, and the TGN marker syntaxin-6, gave *r* values of close to zero, confirming that
213 these markers do not co-localize with UL148. From these results, we conclude that the
214 UL148-dependent ER structures are enriched for cellular markers associated with
215 glycoprotein quality control. In this regard, the UL148 ER structures resemble the "ER
216 quality control (ERQC) compartments" described by G. Lederkremer and colleagues
217 (14, 15, 22). Furthermore, the data indicate that Rh159 cannot substitute for UL148 to
218 induce these structures during HCMV infection of human fibroblasts, nor during RhCMV
219 infection of rhesus fibroblasts (**SI FIG S1**).
220
221 **VCP and Hrd1 are recruited to incipient UL148 ER structures prior to calnexin.**
222 To determine whether there might be differences in the kinetics of recruitment of
223 ERQC markers during formation of the ER structures, we examined a series of time
224 points from one to four days post-infection (dpi) with wild-type HCMV carrying HA-
225 tagged UL148, staining for three different ERQC markers, calnexin, Hrd1, and VCP,
226 alongside UL148 (HA), and acquired results using indirect immunofluorescence
227 confocal microscopy. At 1 dpi the signal from UL148 was only weakly detected, as
228 expected (1), while each of the ER markers was readily detected, providing a read-out
229 of their staining patterns prior to any substantial perturbation by UL148 (**FIG 5**). At 2

230 dpi, we detected robust anti-HA signal, indicating the presence of UL148. At this time
231 point, UL148 exhibited intense signal at small globular puncta, which we interpret to
232 represent incipient UL148 structures, as well as more diffuse staining of a reticular
233 structure consistent with ER. Calnexin (CNX) did not appreciably co-localize with the
234 UL148 puncta until at least 3 dpi, and the structures were not readily visualized from the
235 calnexin channel until 4 dpi (**FIG 5A**). In contrast, signals from Hrd1 and VCP staining
236 were sufficient to mark the UL148 puncta by 2 dpi, which suggests that these markers
237 may co-localize with UL148 at an earlier point during the genesis of the ER structures.
238 Notably, the appearance of Hrd1 at the structures prior to calnexin is consistent with our
239 previous results showing that UL148 co-purifies from infected cells with SEL1L, an
240 adaptor subunit for Hrd1 (8). These results imply that distal elements of the ERAD
241 machinery, exemplified by Hrd1 and VCP, may be recruited to UL148-induced ER
242 structures before calnexin.
243
244 **Visualization of UL148-induced ER structures by electron microscopy.**
245 To discern the ultrastructural appearance of the UL148 structures and to formally
246 ascertain their relationship to the ER, we carried out transmission electron microscopy
247 (TEM) imaging of wildtype (TB_WT) and *UL148*-null (TB_148_{STOP}) infected fibroblasts at
248 5 dpi. In high pressure frozen and freeze-substituted infected fibroblasts, cells with a
249 high density of viral nucleocapsids within the nucleus were selected for analysis, as this
250 feature indicates late time points during infection when UL148 is abundantly expressed.
251 The TEM results revealed prominent globular and oblong structures in the cytoplasm of
252 WT but not of *UL148*-null infected fibroblasts (**FIGS 6-7**). The structures stand out in

253 electron micrographs for their high electron-density, which may reflect the abundance of
254 ERQC proteins together with UL148 in these structures. Under higher magnification,
255 these areas are characterized by accumulations of densely packed ruffled membranes
256 and membranous material, which appear to be collapsed ER. Further, these membrane
257 accumulations were associated with smooth and partially rough ER structures with
258 seemingly enlarged cisternal space. Further, tomographic reconstruction of scanning
259 transmission electron microscopy (STEM) data suggest that densely packed ER
260 cisternae within the structures are interconnected and continuous in three-dimensional
261 space (**FIG 8B-C, SI Movie S1**).
262

263 **A substantial fraction of UL148 is expressed in a detergent-insoluble form during**
264 **infection.**

265 Certain disease-associated mutant alleles of cellular proteins, such as the A103E
266 mutant of the calcium channel Orai1 and the Z-allele of alpha-1 antitrypsin (Z A1AT),
267 localize to anomalous ER structures reminiscent of those we observed here to depend
268 on UL148 (16, 23-26). Furthermore, A103E Orai1 and Z A1AT are found to accumulate
269 in detergent-insoluble forms within the ER, which may represent aggregates or
270 polymers (16, 23, 26), and suggests a mechanism for the formation of ER structures by
271 the proteins. We therefore set out to determine whether differences in detergent
272 solubility between UL148 and Rh159 correlate with their differing potentials to
273 redistribute the ERQC machinery and to cause ER stress (10). To address this
274 question, we infected fibroblasts with TB_148^{HA} or TB_159^{HA} at MOI 1 and at various
275 times post-infection lysed the infected cells in radioimmunoprecipitation assay (RIPA)

276 buffer. After subjecting lysates to high-speed centrifugation, we examined the relative
277 levels of UL148 and Rh159 in the detergent-soluble supernatant and detergent-
278 insoluble pellet fractions.

279 A substantial fraction of UL148 was detected in the detergent-insoluble fractions
280 at all three time points tested (**FIG 9**). However, virtually all of the Rh159 signal was
281 detected in the detergent-soluble fraction. Only when anti-HA antibody signals were
282 shown at high exposure could faint levels of Rh159 be detected in the detergent-
283 insoluble fraction (**FIG 9A**, lower HA panel). From these results we concluded that
284 when compared to Rh159, UL148 is substantially less soluble in a detergent-based lysis
285 buffer, which suggests that UL148 may aggregate or assemble into higher-order
286 structures.

287

288 **UL148 is sufficient to compartmentalize the ER.**

289 Our data thus far demonstrate that UL148 is necessary during infection to cause
290 redistribution of cellular ER markers for glycoprotein quality control processes, such that
291 substantial portion of the ERQC machinery appears to become sequestered away from
292 the rest of the organelle into novel membranous structures. Because a number of viral
293 proteins that remodel the ER during infection are sufficient to alter ER morphology when
294 ectopically expressed [e.g. (27),(28), reviewed in (29)], we wondered whether UL148
295 expression is sufficient to induce ER structures akin to those seen during HCMV
296 infection. Making use of existing “tet-on” ARPE-19 epithelial cells that inducibly express
297 of either UL148 or Rh159, each carrying a C-terminal HA-tag (30), we induced
298 transgene expression for 48 h and subsequently stained for various cellular markers for

299 the ER, for ERQC as well as for LC3B and GABARAP, which are ATG8 family proteins
300 that mark autophagosome membranes.

301 In cells expressing UL148 (i148^{HA}), we observed that calnexin, Hrd1, EDEM1,
302 and VCP co-localize with UL148 at prominent globular structures reminiscent of those
303 observed during infection (**FIG 10**). The respective rough and smooth ER markers
304 ribophorin 1 (RPN1) and reticulon 3 (RTN3), as well as the ATG8 proteins LC3B and
305 GABARAP likewise co-localized to the UL148-induced structures. However, PDI and
306 CALR each failed to co-localize to the structures (**FIG 10**), consistent with our results
307 from infected cells (**FIG 3-4**).

308 In cells expressing the UL148 homolog Rh159 (i159^{HA}), we detected uniform
309 cytoplasmic distribution of ER markers, as well as of HA-tagged Rh159, similar to what
310 we observed during infection with the recombinant HCMV TB_159^{HA} (**FIG 3**). In this
311 setting, the staining patterns for the ATG8 family proteins LC3B and GABARAP failed to
312 indicate any notable structures. Consistent with our previous study showing that UL148,
313 but not Rh159, is sufficient to activate the UPR (10), we observed accumulation of ATF4
314 and phosphorylated eIF2α during induction of UL148 but not Rh159 (**FIG 11A**).
315 Importantly, HA signals indicated that UL148 and Rh159 accumulated at roughly
316 comparable levels following dox induction, which argues against the possibility that
317 gross differences in induced transgene expression accounts for the differences we
318 observed with regard to UPR activation and effects on staining patterns for ER markers.
319 We plotted the Pearson's correlation coefficient to estimate the extent of colocalization
320 between UL148 and various cellular markers: EDEM1, Hrd1, VCP, CNX, RTN3, SEL1L,
321 LC3B, and PDI (**FIG 11B**). The results quantitatively buttress the observations shown in

322 FIG 10. From these results we concluded that no other HCMV gene products are
323 required for UL148 to cause ERQC factors to segregate into discrete compartments,
324 and hence, that UL148 is sufficient to cause large-scale reorganization of ERQC
325 markers. Further, these findings suggested to us that reorganization of ER markers into
326 discrete structures may be related to the propensity of UL148 to induce ER stress.

327 To determine whether UL148-dependent ER remodeling could be visualized in
328 real-time using live cell imaging, we constructed "tet-on" lentiviral vectors that inducibly
329 express either UL148 or Rh159 fused at their predicted C-terminal cytoplasmic tails to
330 the enhanced green fluorescent protein (GFP) from *Aequorea victoria* (31). Following
331 lentiviral transduction, puromycin-resistant ARPE-19 were isolated and subsequently
332 subjected to fluorescence-activated cell sorting (FACS) to enrich for cells that
333 expressed GFP signal following dox treatment. The resulting cell populations, which
334 inducibly express either UL148-GFP or Rh159-GFP, were designated $i148^{GFP}$ and
335 $i159^{GFP}$, respectively.

336 In live cell imaging, we observed that the GFP signal in dox-induced $i148^{GFP}$ cells
337 first appeared in a reticular, largely uniform pattern, which was readily visible at 5 h
338 post-induction. However, by 9 h post-induction punctate structures formed. These
339 puncta progressively grew larger up until the termination of the experiment at 19 h (**FIG**
340 **12A, SI Movie 2**). In contrast, $i159^{GFP}$ cells exhibited a largely diffuse, reticular GFP
341 signal at all post-dox time points monitored (**FIG 12B, SI Movie 3**). The live cell
342 imaging results therefore recapitulated the differences in the HA-staining pattern that we
343 observed between dox-induced $i148^{HA}$ and $i159^{HA}$ cells following fixation, as well as

344 those between HA signals during HCMV infection with TB_148^{HA} and TB_159^{HA} (**FIGS**
345 **1, 3, 10, SI Fig S1**).
346
347 **UL148-GFP structures exhibit poor recovery of fluorescence after**
348 **photobleaching.**
349 To determine whether the protein contents of the UL148 induced structures
350 would exhibit decreased mobility compared to non-perturbed ER, we carried out
351 fluorescence recovery after photobleaching studies. We photobleached regions of GFP
352 signal in i148^{GFP} or i159^{GFP} ARPE-19 cells that had been induced for transgene
353 expression for 24 h and monitored recovery of signal over a 5 min period. In the case of
354 Rh159-GFP expressing cells (i159^{GFP}), fluorescence almost fully recovered within 3 min
355 (**FIG 13**). In contrast, when we photobleached a prominent UL148-GFP structure, the
356 GFP signal failed to appreciably recover fluorescence over the 5 min period for which
357 we obtained measurements. Nonetheless, an area of reticular GFP signal in an i148^{GFP}
358 cell, which presumably represented an ER region not involved in an anomalous ER
359 structure, recovered fluorescent signal with kinetics similar to those observed during
360 Rh159-GFP expression. These results suggested to us that UL148 structures do not
361 exchange their contents as efficiently as unperturbed ER, or that at least the UL148-
362 GFP within the structures is not able to be replaced rapidly with UL148-GFP protein
363 from other parts of the cell.
364
365
366 **Ectopically-expressed UL148 is degraded by proteasomes and not by autophagy.**

367 Although the UL148 ER structures were found to be enriched with proteins such
368 as Hrd1, SEL1L, EDEM, and VCP (**FIG 3-4**, **10-11B**) that are posited to play key roles in
369 ERAD, a process during which misfolded glycoproteins are recognized, processed, and
370 dislocated across the ER membrane for degradation at cytosolic proteasomes, we had
371 also obtained evidence suggesting that elements of the machinery for autophagy also
372 associated closely with the UL148 structures. Namely, the mammalian ATG8 ortholog
373 GABARAP co-localized with UL148 during infection (**FIG 3-4**), and both GABARAP and
374 another ATG8 ortholog, LC3B, both localized with the ER structures induced during
375 ectopic expression of UL148 (**FIG 10, 11B**). Therefore, we wished to determine
376 whether UL148 would degraded by the proteasome, as would be consistent with
377 conventional ERAD, or by the lysosome, which would suggest a functional role for
378 autophagy-related processes, such as selective autophagy of the ER (32), in dispensing
379 with UL148.
380 As a first step, we conducted a live-cell imaging "washout" experiment in which
381 $i148^{GFP}$ cells were induced for transgene expression for 24 h, after which the growth
382 medium containing inducing agent (dox) was removed, the cells were washed, and then
383 the medium was lacking the inducing agent was applied to the cells. During a 22 h
384 imaging period following dox-washout, we observed the structures to become
385 progressively smaller as the reticular and punctate GFP signals abated (**FIG 14A, SI**
386 **Movie S7**). Because the results suggested that UL148-GFP structures could be
387 resolved over time, we induced UL148-GFP in tet-on ARPE-19 cells ($i148^{gfp}$) for 24 h,
388 washed out the inducing agent (dox) and then applied either epoxomicin (20 μM), an
389 irreversible inhibitor of the proteasome (33), or folimycin (115 nM), a proton pump

390 inhibitor that blocks autophagosome maturation and impedes the lysosome-dependent
391 protein degradation (34, 35). Of the two inhibitors, only epoxomicin markedly stabilized
392 UL148, as evidenced by Western blot signal for both GFP and UL148 (**FIG 14B-C**).
393 Folimycin had no obvious effect on UL148-GFP levels, even though the drug led to
394 increased levels of LC3B-II, as expected. From these results, we conclude that
395 ectopically expressed UL148 is primarily degraded by a proteasome-dependent
396 mechanism.
397
398 **UL148 requires the integrated stress response to cause ER reorganization.**
399 We previously defined that UL148 triggers the UPR during ectopic expression,
400 and that UL148 contributes to activation of the PKR-like ER kinase (PERK) and inositol
401 requiring enzyme 1 (IRE1) during infection (10). Although we failed to find any effect of
402 small interfering RNA (siRNA) or drug treatments targeting IRE1 on UL148-dependent
403 ER remodeling (not shown), we did observe that siRNA directed at PERK caused
404 UL148 to fail to form puncta or to co-localize with Hrd1 (not shown). Furthermore, the
405 literature suggests that formation of ERQC compartments requires PERK (36). PERK
406 responds to ER stress by activating the integrated stress response (ISR). PERK
407 activates the ISR by phosphorylating eIF2α at Ser51 (eIF2α-P); in turn, the
408 accumulation of eIF2α-P causes global attenuation of mRNA translation whilst
409 paradoxically stimulating translation of select mRNAs, such as those encoding ATF4
410 and CHOP, which play roles in adaptation to stress (37). Stress-regulated translation of
411 such mRNAs involves small upstream open reading frames, termed uORFs, in their 5'
412 untranslated regions that ordinarily suppress translation under basal conditions (38, 39).

413 To examine whether ER remodeling in response to UL148 requires the ISR, we
414 turned to a well characterized small molecule inhibitor of stress-regulated translation,
415 ISRIB (40-44). ISRIB is thought to function by acting as a "molecular staple" that holds
416 the guanine nucleotide exchange factor eIF2B in an active decameric configuration (42-
417 45), such that eIF2B will continue to generate ternary complex (eIF2•GTP•Met-tRNAi)
418 necessary for new cycles of translational initiation, despite the presence of phospho-
419 eIF2α (Ser51). Because PERK is the kinase that phosphorylates eIF2α in response to
420 ER stress (46, 47), we also tested for effects of the PERK inhibitor GSK2606414 (48).
421 Having confirmed that ISRIB and GSK260641 failed to negatively impact UL148
422 expression in dox-induced i148^{HA} cells, when the drugs were applied at 200 nM or 1.1
423 μM, respectively **(FIG 15A-B)**, we treated i148^{GFP} cells with 200 nM ISRIB, 1.1 μM
424 GSK260641, or DMSO vehicle control, and carried out live cell imaging during dox
425 induction of UL148-GFP.
426 Strikingly, ISRIB and GSK6060414 virtually abolished the formation of UL148
427 puncta through 13 h post induction (dox addition), a time point at which the DMSO
428 control condition showed abundant large structures (**FIG 15C-E, SI Movies 8-10**).
429 Based on our previous findings (**FIGs 1-3, 6-7, 10)**, we interpret the formation and
430 subsequent large-scale aggregation of UL148-GFP puncta as a faithfully indicator of ER
431 remodeling in response to UL148. Therefore, these results suggested to us that
432 pharmacological treatments that inhibit the ISR and PERK prevent UL148 induced
433 remodeling of the ER, which further implies that ER remodeling in response to ER
434 stress requires stress-regulated translation.
435

436 Since our results with ISRIB and GSK6060414 during ectopic expression of
437 UL148 suggested that the ISR is required for UL148 mediated ER-remodeling, we next
438 asked whether these pharmacological agents would prevent UL148-dependent ER
439 remodeling in the authentic context of the HCMV infected cell. In live cell imaging
440 studies with ISRIB and GSK6060414, UL148-GFP puncta began to appear by ~17 h
441 post treatment (**FIG 15D-E, SI Movies 9-10**), suggesting that the inhibitory effects of the
442 drugs diminish over time. To ensure that the inhibitory activity would be maintained
443 over a four-day time course study in HCMV infected cells, we replaced the media at
444 each 24 h interval following infection to replenish freshly reconstituted ISRIB,
445 GSK6060414, or DMSO vehicle control.
446 Formation of ER structures was virtually ablated at 4 dpi during infection with
447 either ISRIB or GSK2606414 (**FIG 16A**). We used Imaris 3D imaging analysis of at
448 least 30 cells per condition to calculate the percentage of Hrd1 signals that coalesced
449 into discrete structures during infection, and the results corroborated statistically
450 significant differences between the DMSO carrier alone setting compared to treatments
451 with either GSK2606414 or ISRIB (**FIG 16B**). Furthermore, Western blot results
452 indicated roughly similar levels of UL148 in drug treated and DMSO control conditions,
453 and that ISRIB and GSK2606414 treatments both caused reduced levels of ATF4, while
454 PERK inhibitor alone was able to reduce the levels phospho-eIF2α (Ser51), detected by
455 a phospho-specific antibody, as expected (**FIG 16C-D**). A modest reduction, however,
456 was observed for the levels of viral envelope glycoprotein B (gB) during ISRIB and
457 GSK2606414 treatments, which suggests that the ISR may be required for optimal
458 expression of the certain viral envelope glycoproteins. Indeed, even viruses lacking

459 *UL148* cause high levels of ATF4 accumulation at late times during infection, a time
460 when viral late genes, such a gB, are expressed at high levels (10). Regardless,
461 because the PERK inhibitor and ISRIB each prevented the appearance of discrete
462 UL148 ER structures while failing to substantially affect UL148 expression, these results
463 were consistent with those from our ectopic expression studies. Taken together, our
464 findings argue that the ISR is required for redistribution of ERQC markers in response to
465 UL148.

466 **DISCUSSION**

467 The ER structures we have identified herein are notable in several regards.
468 Firstly, this example of virally-induced ER remodeling is wholly dependent on a single
469 viral gene product, UL148. Of course, there are other examples of individual viral gene
470 products that are necessary to grossly perturb ER morphology during infection and
471 sufficient to induce such perturbations during ectopic expression [e.g., (27, 28, 49, 50)]
472 Nonetheless, to the best of our knowledge the ER structures caused by UL148 are a
473 hitherto undescribed ultrastructural characteristic of the HCMV infected cell, which is
474 surprising given their size, scale, and prominence. Indeed, the average volume of the
475 structures at 96 h postinfection amounts to roughly 60% of the size of the nucleus of an
476 uninfected human fibroblast [~500 μm^3, (51)]. Although UL148 expression is
477 accompanied by UPR activation, ER reorganization occurs without killing the host cell,
478 even in the setting of ectopic expression when viral functions that inhibit programmed
479 cell death are absent. Nor do we see any effects of UL148 on the yield of infectious
480 virus during replication in fibroblasts, since *UL148*-null mutant viruses replicate
481 indistinguishably from wildtype parental virus in cultured cells (1, 8). As with all
482 enveloped viruses, HCMV requires the host cell secretory pathway to fold and process
483 enormous quantities of viral envelope glycoproteins that endow progeny virions with the
484 molecular machinery for infectivity. It is intriguing to consider how the infected cell
485 tolerates spatial reorganization of ER membranes and the associated glycoprotein
486 quality control machinery without any overtly impact on the production of infectious
487 progeny virions.

488 Furthermore, certain aspects of ER reorganization invoked by UL148 may be
489 novel to cell biology. In particular, the densely packed collapsed ER in close
490 association with varicosities that we observe to depend on UL148 during infection
491 appear to differ from the ER structures caused by other ER perturbagens. For instance,
492 a hereditary form of childhood cirrhosis caused by the *Z* allele of the alpha-1-antitrypsin
493 (Z-A1AT) gene (*SERPINA*) is characterized by polymerization of Z-A1AT within the ER
494 (25), leading to its accumulation in membrane-delimited inclusions (25, 26, 52).
495 However, Z-A1AT inclusions are not observed to associate with regions of collapsed
496 ER, nor does Z-A1AT suffice to activate the UPR, even though its expression does
497 sensitize cells to other triggers of ER stress (26, 53).
498 HCMV encodes at least one other ER-resident immunevasin implicated to
499 activate the UPR, US11 (54). While UL148 binds the NK-cell and T-cell costimulatory
500 ligand CD58 to prevent its transport to the cell surface, US11 targets the heavy chain of
501 class I major histocompatibility complex (MHC) for ER-associated degradation (55, 56).
502 While UL148 retains CD58 in the ER and causes it to accumulate in presumably
503 immature glycoform that migrates with enhanced mobility in SDS-PAGE, there is no
504 obvious decrease in the overall abundance of CD58 (9). Even though intracellular
505 forms of CD58 in our hands are refractory to detection by indirect immunofluorescence
506 (not shown), we hypothesize that UL148 sequesters CD58 into the unusual ER
507 structures. Further, our detergent solubility results are consistent with the notion that
508 UL148 may form aggregates or polymers in the course of preventing CD58 presentation
509 at the cell surface (FIG 9). It is intriguing UL148, an immunevasin targeting CD58,
510 induces dramatic morphologic rearrangements of the ER, while another HCMV

511 immunevasin, US11, targeting MHC class I for degradation fails to do so, even though
512 both trigger ER stress. Although we cannot yet exclude the possibility, it is plausible
513 that retention of CD58 is required for ER reorganization.

514 While relationship between the mechanism for CD58 retention and the formation
515 of UL148-dependent ER structures remains unresolved, our findings suggest a
516 mechanism to explain the influence of UL148 on HCMV cell tropism. Because we find
517 that UL148 causes sequestration of the ER mannosidase EDEM1 and the basal E3
518 ubiquitin ligase SEL1L/Hrd1 into large membranous structures, regions of rough ER not
519 drawn into the structures might be expected to offer a more permissive folding
520 environment for poorly folding polypeptides that otherwise would be more efficiently
521 targeted for ERAD. Indeed, our results also indicate that the reticular ER, as indicated
522 by the staining pattern for calreticulin, PDI, and KDEL antibodies, remains largely intact
523 following UL148-induced ER reorganization of ER quality control markers into discrete
524 structures. Based on these observations, we hypothesize that UL148-mediated
525 sequestration of the glycoprotein quality control machinery alters the proteostatic
526 environment of the ER by physically dislocating key elements of the “mannose removal
527 time clock” (57, 58) that marks substrates for ERAD from marking said substrates for
528 destruction. Since glycoprotein O (gO) is at once a constitutive ERAD substrate (1, 8)
529 and a core component of a viral envelope glycoprotein complex that governs HCMV
530 entry and cell tropism (5-7, 59, 60), the hypothesis does not seem unreasonable on its
531 face. Obviously, however, it will be crucial to determine whether any generic ERAD
532 substrate are stabilized during UL148 expression, as would be predicted by this model.

533 Although many of the ERQC markers that co-localize with UL148 at the ER
534 structures, such as Hrd1 and EDEM1, are understood to play roles in pathways that
535 control proteasome dependent ERAD of terminally-misfolded glycoproteins, the
536 observation that GABARAP localizes to the structures during infection, and that both
537 LC3 and GABARAP do so during ectopic expression may suggest roles for autophagy-
538 related pathways in ER reorganization. However, our results indicate that UL148 is
539 degraded by a proteasome-dependent pathway and not by lysosomes. Therefore, it
540 seems unlikely that selective autophagy of the ER is involved in recycling or degrading
541 these ER structures. Nonetheless, our live cell imaging results suggest that the UL148
542 ER structures originate as puncta that traffic to accumulate into larger structures, which
543 may suggest a relevance for co-localization with ATG8 family proteins. Previous
544 studies have shown that misfolded proteins traffic in a microtubule (MT)-dependent
545 manner to form pericentriolar structures termed aggresomes (61, 62). ATG8 family
546 proteins such as LC3B not only play roles in degradation of substrates via
547 macroautophagy, but also bind MTs and recruit machinery for MT-dependent transport
548 of cargos (63-65). Therefore, it seems likely that the occurrence of GABARAP and
549 LC3B at the UL148 ER structures indicates recruitment of cellular machinery that
550 transports perturbed regions of ER to sites of large-scale accumulation.
551 Despite that our results indicate that the ISR is required for ER reorganization
552 during UL148 expression, precisely how UL148 triggers ER stress remains unknown.
553 UL148 has been found to co-purify from cells with SEL1L, a component of the ERAD
554 machinery. Thus, it seems plausible that UL148 may inhibit the Hrd1/SEL1L complex,
555 which would be predicted to cause the buildup of unfolded protein and thus trigger the

556 UPR. However, inhibition of ERAD alone seems unlikely to account for the formation of
557 ER structures. Another non-mutually exclusive possibility is that UL148 multimerizes in
558 a manner that constricts the ER lumen. Although the mechanism remains highly
559 speculative, the assembly UL148 molecules on opposite sides of the ER lumen might
560 constrict the organelle in a manner consistent with our EM results (FIG 6, 8).
561
562

563 **MATERIALS AND METHODS.**

564

565 **Cells and Virus.**

566 hTERT-immortalized human foreskin fibroblasts (8), derived from ATCC HFF-1 cells
567 (SCRC-1041) were maintained in Dulbecco's modified Eagle's medium supplemented
568 with 5%-10% newborn calf serum (Millipore Sigma) and antibiotics (complete DMEM)
569 exactly as described previously (8). i148^{HA} and i159^{HA} ARPE-19 epithelial cells (10),
570 which upon treatment with 100 ng/mL doxycycline, express HA-tagged UL148 or
571 Rh159, respectively, were likewise maintained in complete DMEM. For live cell imaging
572 studies, i148^{HA} and i159^{HA} ARPE-19 were maintained in Opti-MEM (Thermo Fisher)
573 supplemented with 3% certified tet-approves fetal bovine serum (FBS), 20 µg/mL
574 gentamicin sulfate, 1 µg/mL puromycin HCl and 10 µg/mL ciprofloxacin HCl.
575 Telomerase-immortalized rhesus fibroblasts (66) were a kind gift of Peter A. Barry, and
576 were maintained in complete DMEM. The acute monocytic leukemia cell line THP-1
577 (TIB-202) was obtained from ATCC (Manassas, VA) and were maintained in RPMI 1640
578 medium supplemented with 10% FBS (Millipore Sigma) and antibiotics (10 µg/mL
579 ciprofloxacin and 25 µg/mL gentamicin). Prior to infection with HCMV THP-1 were
580 differentiated into adherent macrophages by treatment with the phorbol ester, 2-O-
581 tetradecanoylphorbol 13-acetate (Millipore Sigma).

582

583 Infectious bacterial artificial chromosome (BAC) clones of HCMV strain TB40/E (also
584 known as TB40-BAC4 or TB_WT)(67), of strain TR (TR*gfp*)(68, 69), of strain Merlin

585 repaired for *UL128* and *RL13* harboring *tetO* sequences upstream of *UL131* (pAL1393)
586 (70), and of rhesus CMV strain 68-1 (71) were used in this study.
587
588 **Construction of recombinant viruses and recombinant DNAs.**
589 The TB40-BAC4 derivatives TB_148^{HA} and TB_148$_{STOP}$ were used in our previous
590 studies and are described therein (1, 8, 10). New recombinant HCMVs for this study
591 were derived from BAC-cloned HCMV and RhCMVs using *en passant* mutagenesis in
592 GS1783 *E. coli,* a strain K12 derivative that expresses the homing endonuclease I-SceI
593 upon treatment with L-(+)-arabinose (72, 73). Recombinant BACs were confirmed by
594 Sanger DNA sequencing of the modified regions by Genewiz (Piscataway, NJ) (not
595 shown). Oligonucleotide primers for construction of recombinant viruses and plasmids
596 were custom synthesized by Integrated DNA Technologies (Coralville, IA); sequences
597 are provided in **Table S1**. Restriction enzymes, T4 DNA ligase, and Gibson assembly
598 reagents (NEB HiFi Assembly Master Mix) were obtained from New England Biolabs
599 (Ipswitch, MA).
600 To construct TB_159^{HA}, a strain TB40/E derivative in which the UL148 open
601 reading frame is replaced by Rh159 we carried out the following steps. Primers
602 Rh159_Fw and Rh159_HA_Rv were used to amplify and HA-tag the *Rh159* ORF from
603 pcDNA3.1+_Rh159_IRES_GFP (a gift from Klaus Früh, OHSU). The PCR product was
604 inserted into EcoRV-digested pEF1α using Gibson assembly. A PCR product
605 containing an ISce-I excisable kanamycin cassette was amplified from TB_148^{HA}_*ISce-*
606 *Kan* integrate BAC (1) using primers PpuISceKanGibs_Fw and PpuISceKanGibs _Rv
607 and Gibson-assembled into PpuMI-digested pEF1α_Rh159 plasmid to yield plasmid

608 pEF1α_Rh159_ISceKan. Primers Rh159_Fw_recomb and Rh159_Rv_recomb were
609 used to generate a PCR product from template plasmid pEF1α_Rh159_ISceKan. The
610 PCR product was electroporated into GS1783 E. coli harboring the TB_148^{HA} BAC, and
611 Kan^{r} colonies harboring TB_Δ148_Rh159_ISceKan integrate BACs were isolated on
612 Luria-Bertiani agar plates. Bacterial colonies representing Kan resistant integrates were
613 obtained, and integrates were subsequently resolved using standard *en passant*
614 protocols to yield TB_Δ148_Rh159^{HA}, which we abbreviate herein as TB_159^{HA}.
615 TB_159^{HA} was sequence-confirmed using primers TB_Rh159HA_seq_Fw and REV
616 TB_Rh159HA_seq. Similar strategies were used to modify the RhCMV 68-1 BAC (71)
617 so as to insert sequences encoding the nonapeptide HA-epitope such that Rh159 would
618 be expressed from the virus carrying a C-terminal HA tag. An *en passant* strategy in
619 which a shuttle plasmid carrying *I-SceI-Kan^{r}* disrupted by in-frame nonsense codons
620 was used insert premature nonsense codons in the *UL148* CDS in the context of HCMV
621 strains Merlin (pAL1393) and TR (TR*gfp*), and was applied as described previously for
622 generating TB_148$_{STOP}$, the UL148$_{STOP}$ mutant of strain TB40/E (8).
623 To construct "tet-on" lentivirus vector plasmids containing UL148 fused to GFP,
624 we used primers Gibs_eGFP_Rv and 148_eGFP_Fw to amplify the GFP gene from a
625 dsDNA gBlock, EGFP-P2A-3XHA, synthesized by Integrated DNA Technologies, gift of
626 Matthew D. Woolard, LSUHSC-S. In a separate PCR, the *UL148* gene was amplified
627 from plasmid pcDNA3.1-UL148^{HA} (10) using primers Gib_148_Fw
628 148_noStopRv. The two products were assembled together with EcoRV opened
629 pcDNA3.1(+) (Invitrogen) to produce pcDNA3.1-UL148-GFP. After confirming the
630 absence of spurious mutations by Sanger DNA sequencing (Genewiz), the *UL148-GFP*

631 cassette from pcDNA3.1-UL148-GFP was released by EcoRI and NotI digestion and
632 ligated into pOUPc turboRFP-link plasmid which had been linearized using the same
633 restriction sites. pOUPc turboRFP-link is a derivative of lentiviral vector pOUPc (10)
634 that was constructed by reinsertion of turboRFP (tRFP). Briefly, tRFP was amplified
635 from the original pOUPc-turboRFP using primer pair tRFP linker Fw and tRFP linker Rv
636 and then reinserted by Gibson Assembly with pOUPc turboRFP that had been double-
637 digested using EcoRI and Not I in order to linearize the vector and remove the
638 *turboRFP* (RFP) sequence. To express Rh159 fused to GFP, primers Gibs_eGFP_Rv
639 and 159_eGFP_Fw were used to amplify the GFP gene from EGFP-P2A-3XHA, and in
640 a separate PCR reaction, primers Gibs_159_Fw and 159_noStop_Rv Rh159 were
641 used to amplify *Rh159* from pcDNA3.1-Rh159^{HA} (10). The latter two PCR products were
642 assembled together with EcoRV linearized pcDNA3.1(+) using Gibson Assembly,
643 resulting in plasmid pcDNA3.1-Rh159. The latter plasmid was used as template in a
644 PCR reaction with primers Gibs_Age_159_Fw and Gibs_Mlu_GFP_Rv. The resulting
645 PCR product was Gibson assembled into the lentiviral vector pOUPc (10) which had
646 been double-digested with Mlu I and Age I.
647
648 **Drug treatments.**
649 The PERK inhibitor, GSK2606414 (48), doxycycline hyclate, and folimycin were
650 obtained from MilliporeSigma (Burlington, MA). ISRIB (40-44) was obtained from
651 MilliporeSigma or APExBio (Boston, MA) and epoxomicin was procured Selleck
652 Chemicals (Houston, TX). ISRIB was dissolved in DMSO and used at a final
653 concentration of 200 nM in live cell imaging and HCMV infection experiments but was

654 used at 2 μM in Western blotting experiments with i148^{HA} ARPE-19 cells to address
655 whether the drug interfered with UL148 expression. GSK2606414 was also dissolved in
656 DMSO and used at a final working concentration of 1.1 μM. Folimycin was prepared as
657 a 1000× (115.46 μM) stock solution in DMSO and used at 115 nM final. Epoxomycin
658 was prepared as a 100× (2 mM) stock solution in DMSO and used at a final
659 concentration of 20 μM.
660
661 **Confocal Microscopy and Live Cell Imaging.** Confocal indirect immunofluorescence
662 microscopy imaging on fixed cells was carried out using Leica TCS SP5 Spectral
663 Confocal Microscope (Leica Microsystems, Heidelberg, Germany) using a Leica HCX
664 PL APO CS 63x/1.4-0.6NA objective under oil immersion, except for the image shown
665 in Figure 1C, which was captured on a Nikon SIM-E and A1R confocal microscopy
666 system (Nikon Instruments, Melville, NY) using a Nikon SR Apo TIRF 100x/1.49NA
667 objective under oil immersion. Images for different fluorophore channels were acquired
668 using sequential scanning. Direct immunofluorescence live cell imaging data were
669 collected using the Nikon SIM-E microscope using a Nikon Apo 60x/1.40NA DIC
670 objective.
671 The 3D projections shown in FIGs 1D and 16A were generated from Z-stacks
672 captured on the Nikon SIM-E / A1R microscope using a Nikon SR Apo TIRF
673 100x/1.49NA objective. For FIG 1D, the 3D projection was generated using NIS-
674 Elements AR Analysis 4.60.00 (64-bit) software (Nikon). For FIG 16A, 3D projections
675 were generated by Imaris x64 9.3.0 software (Bitplane, Inc.) in maximum intensity
676 projection (MIP) mode.

677 For fixed cell imaging experiments other than those shown in Fig S1 panels E, F,
678 G, and H, cells were seeded on 12 mm circular, No. 1 thickness microscope cover glass
679 (200121; Azer Scientific, Morgantown, PA). At the indicated times post-treatment and or
680 post-infection, cells were washed with phosphate buffered saline (PBS) [137 mM NaCl,
681 2.7 mM KCl, 10 mM Na_2HPO_4, and 1.8 mM KH_2PO_4, pH 7.4]; fixed for 15 min at room
682 temperature in PBS containing 4% (wt/vol) paraformaldehyde (Fisher Scientific, Waltham,
683 MA), washed in PBS, permeabilized for 10 min using 0.1% Triton X-100 (in PBS),
684 subsequently washed again in PBS, and then blocked for 45 min at 37 °C in PBS
685 containing 5% (vol/vol) normal goat serum (Rockland Immunochemicals, Limerick, PA).
686 Cells were then washed three times in PBS followed by incubation in 1% Human Fc Block
687 (BD Biosciences, San Jose, CA) in PBS, for additional 45 min at 37 °C. Cells were then
688 incubated in the presence of primary antibodies for 1 h at 37 °C or 4 °C overnight, and
689 then washed three times with PBS containing 0.1% Tween-20 (PBST) for 5 min per wash.
690 Alexa Fluor-labeled goat polyclonal secondary antibodies (all from ThermoFisher
691 Invitrogen, Waltham, MA, see **Table S2**) were used for secondary detection. The slides
692 were then mounted using Prolong Gold anti-fade reagent containing DAPI
693 (ThermoFisher) and placed under a Leica TCS SP5 confocal microscope for image
694 acquisition using a Leica 63× oil immersion objective lens (Leica Microsystems, Buffalo
695 Grove, IL).

696 For indirect immunofluorescence staining results of primary clinical isolates (SI Fig
697 S1 panels E-H), four clinical HCMV isolates obtained by routine testing of throat swabs
698 from patients of the Ulm University Medical Center were provided by the diagnostic
699 laboratory of the Institute of Virology in Ulm. Sample material was applied to human

700 fibroblasts and incubated for several days until HCMV-positive cells could be detected.
701 Infected cells were then seeded together with uninfected fibroblasts, incubated for up to
702 5 days until plaques were formed and processed for indirect immunofluorescence
703 staining. ERQC compartments were detected by staining for calnexin (CNX, E10; Santa
704 Cruz Biotechnology, mouse, 1:50 dilution), the cVAC was detected by staining for HCMV
705 pUL71 (rabbit, 1:500). Secondary antibody used for detection of CNX was Alexa Fluor
706 555 labeled goat anti-mouse IgG (1:1000) and for pUL71 detection, Alexa Fluor 488
707 conjugated goat anti-rabbit IgG (1:1000). Confocal images were acquired using the 63×
708 objective of a Zeiss Observer Z1 fluorescence microscope equipped with Apotome and
709 Zen software 2.3 (Carl Zeiss Microscopy GmbH, Jena, Germany).
710
711 **FRAP.** FRAP studies were carried out on using live ARPE-19 cells from the i148^{GFP}
712 and i159^{GFP} populations as follows. Cells were seeded as above for live-cell imaging,
713 induced for transgene expression using dox (100 ng) for 24 h, and then placed on an
714 incubated sample stage of a Nikon A1R SIM-E imaging system equipped with an SR
715 Apo TIRF 100x/1.49NA objective (Nikon). Three rectangular regions in image fields
716 were defined for measurement of (i) background signal, and of two regions with
717 comparable initial GFP signals, (ii) one designated as a control region (no
718 photobleaching) and another for (iii) photobleaching and recovery of signal after
719 photobleaching. Photobleaching of selected regions was carried out for 20 s using 405
720 nm laser light from a LU-N4 laser fiber (Nikon) [power at source: 15 mW, at objective: 8
721 mW]. Images and signal intensity measurements were captured every 2 s at a rate of 1

722 frame per s (488 nm excitation, FITC channel) starting immediately before
723 photobleaching (t=1), and from t=20 s to t=320 s after.
724
725 **Electron Microscopy.** Procedures to prepare samples for transmission electron
726 microscopy (TEM) included high-pressure freezing (HPF), freeze substitution, and Epon
727 embedding, which were carried out as described previously (74). Briefly, human
728 fibroblasts were seeded in µ-Slides (Ibidi GmbH, Martinsried, Germany) containing
729 carbon-coated sapphire discs (Engineering Office M. Wohlwend GmbH) 1 day prior to
730 infection at 80 to 90% confluence. Cells were infected with virus overnight at MOI 1.
731 Medium containing viral inocula was replaced with fresh medium the next day. Infected
732 cells on sapphire discs were fixed by using HPF with a Compact 01 high-pressure freezer
733 (Engineering Office M. Wohlwend GmbH, Sennwald, Switzerland) at 5 dpi. Thereafter,
734 cells on sapphire discs were processed by freeze-substitution and subsequently
735 embedded in Epon (Fluka, Buchs, Switzerland). Ultrathin sections of the Epon-embedded
736 cells were cut with an ultramicrotome (Ultracut UCT; Leica Microsystems, Wetzlar,
737 Germany) and placed on Formvar-coated single-slot grids (Plano GmbH, Wetzlar,
738 Germany). Grids were examined in a Jeol JEM-1400 (Jeol Ltd., Tokyo, Japan)
739 transmission electron microscope equipped with a charge-coupled-device (CCD) camera
740 at an acceleration voltage of 120 kV. Fixation and embedding of infected cells for
741 scanning transmission electron microscopy (STEM) tomography was the same as
742 described for TEM. Additional sample preparation steps were conducted as described
743 previously (75, 76). Tomogram acquisition was conducted on a STEM Jeol JEM-2100F
744 with an acceleration voltage of 200 kV. Tilt series were acquired from 600 nm thin sections

745 from +72° to -72° with a 1.5° increment using the bright field detector. Image series were
746 reconstructed to tomograms by weighted back projection with the IMOD software
747 package (77). Three-dimensional visualization of the membrane structures was
748 performed using Avizo lite software (Visualization Science Group, Burlington, MA, USA)
749 by threshold segmentation.
750
751 **Western blotting.** Western blotting procedures, including primary and secondary
752 antibodies used for detection of HA tag, ATF4, eIF2α, P-eIF2α (Ser51), the HCMV viral
753 nuclear antigen IE1, and the conditions used for detection of Ser51 phosphorylated
754 eIF2α, were carried out as described previously (8, 10). Additional antibodies used in
755 this study were mouse anti-GAPDH (Cat. No. 60004-1, Proteintech, Rosemont, IL,),
756 mouse anti-gB clone 27-180 (78) (a generous gift of William J. Britt), and anti-GFP
757 (D5.1) XP® Rabbit mAb #2956 (Cell Signaling Technology, Danvers, MA).
758
759 **Statistical analyses.** Statistical analyses were carried out using GraphPad Prism 8.1.0
760 for MacOS (GraphPad, San Diego, CA).
761
762 **ACKNOWLEDGEMENTS.**
763 This project was supported by NIH grants R01-AI116851 (to J.P.K.) and P30-
764 GM110703. Its contents are solely the responsibility of the authors and do not
765 necessarily represent the official views of the NIAID.
766 We are grateful to Erik L. Snapp (HHMI, Janelia Laboratories) for helpful
767 discussions concerning EM and confocal image data. We also thank Jacob E. Corn

768 and Jin Rui “Amos” Liang (both of ETH Zurich, Switzerland), Dong Yu (Washington
769 University, St. Louis, MO, currently GSK Vaccines), Thomas E. Shenk (Princeton
770 University, Princeton, NJ), Richard J. Stanton (Cardiff University, United Kingdom),
771 William J. Britt (University of Alabama, Birmingham), W. L. William Chang and Peter A.
772 Barry (both of the University of California, Davis; Davis, CA), Christian Sinzger
773 (University Medical Center Ulm, Ulm, Germany), Klaus Früh (Oregon Health Sciences
774 University, Beaverton, OR), and Gregory A. Smith (Northwestern University, Chicago,
775 IL) for generously sharing reagents.
776

777 **FIGURE LEGENDS:**

778

779 **FIG 1. UL148 reorganizes ER markers into anomalous structures during HCMV**
780 **infection.**

781 Fibroblasts infected at 1 MOI with either **(A)** wildtype HCMV strain TB40/E (TB_WT) or
782 **(B)** an isogenic *UL148*-null mutant (TB_148$_{STOP}$), were fixed at 96 h postinfection (hpi)
783 and imaged by confocal microscopy after staining with antibodies specific for CNX or Hrd1
784 (magenta) and glycoprotein H (gH, green), as indicated. DAPI (blue) signal was used to
785 counterstain nuclei. **(C)** Percentage of fibroblasts that contain Hrd1 structures at 96 hpi,
786 Fifty gH-positive cells for each condition were scored for presence or absence of UL148
787 structures (also see SI Fig S1A). (**D**) Three-dimensional confocal image projection of a
788 TB_WT infected fibroblast stained at 96 hpi for Hrd1 and gH. **(E)** Volumetric
789 measurements were made from sixteen infected cells, stained with phalloidin-AlexaFluor
790 594 conjugate to estimate total cell volume, with Hrd1 antibody to estimate the volume of
791 UL148-dependent ER structures, and with DAPI to estimate nuclear volume.

792

793 **FIG 2. Characterization of TB_148^{HA} and TB_159^{HA} viruses. (A)** Human fibroblasts
794 were infected at MOI 1 with the indicated recombinant HCMVs and whole cell lysate
795 samples harvested at the indicated times post-infection (h post-infection: hpi) were
796 analyzed by Western blot to detect HA-tagged UL148 or Rh159, the 72 kD viral nuclear
797 antigen IE1-72 (IE1), and GAPDH. **(B)** Single-cycle viral replication kinetic curves from
798 MOI 1 infected fibroblasts were plotted by determining the titer in tissue culture infectious
799 dose 50 ($TCID_{50}$) from supernatants collected at the indicated times postinfection.

800

801

802 **FIG 3. UL148 localizes to unusual ER compartments enriched for glycoprotein**
803 **quality control markers.** Fibroblasts infected at MOI 1 with either TB_148^{HA} (panels: **A,**
804 **C, E, G, I, K, M, O, Q, S**) or TB_ 159^{HA} (panels: **B, D, F, H, J, L, N, P, R, T**) were fixed
805 at 96 hpi, and imaged by confocal microscopy after co-staining with antibodies specific
806 for HA (UL148/Rh159, magenta in merge) and the indicated cellular markers (green in
807 merge). DAPI (blue) counterstaining is shown in merged image.

808

809 **FIG 4. Quantification of Co-localization between UL148 and Cellular Markers.** A
810 Pearson's correlation coefficient (*r*) was calculated using NIH ImageJ software to estimate
811 the degree of co-localization between UL148 (HA signal) and each of the indicated
812 cellular markers. A minimum of 30 cells were analyzed per marker. The arithmetic mean
813 for each co-localization analysis result is shown as a blue line, and data points for
814 individual cells analyzed are plotted as circles.

815

816 **FIG 5. Cellular proteins involved in glycoprotein quality control are recruited with**
817 **differing kinetics to UL148 ER structures.** Fibroblasts infected with TB_148^{HA} at 1 MOI
818 were fixed at the indicated time points (days post infection, dpi) and imaged by confocal
819 microscopy after staining with antibodies specific for HA (UL148, magenta), CNX (green,
820 **A**) , Hrd1 (green, **B**) or VCP(green, **C**), DAPI (blue).

821

822 **FIG 6. TEM of ER structures in wild-type HCMV infected cells.** Human fibroblasts
823 infected with wildtype HCMV (TB_WT) were fixed by high-pressure freezing and freeze
824 substitution at day 5 postinfection and imaged using TEM. Panels (**A**) and (**B**) show cell
825 overview at left. For each cell, the boxed region is shown at higher magnification.
826 Scale bars; left panels: 10 µm, right panels: 2 µm. rER: rough ER; Nu: nucleus; cVAC:
827 cytoplasmic viral assembly compartment. Solid arrowheads indicate the UL148-
828 dependent ER structures of interest.
829
830 **FIG 7. TEM of *UL148*-null HCMV infected cells.** Human fibroblasts infected with a
831 *UL148*-null mutant (TB_148STOP) were fixed by high-pressure freezing and freeze
832 substitution at day 5 postinfection and imaged using TEM. At the upper left an overview
833 panel of a representative cell is shown with panels **A, B, and C** each boxed. The boxed
834 regions are expanded at higher magnification at right (**A**) and below (**B, C**). Scale bars
835 for upper left overview panel: 10 µm, for zoomed panels: 2 µm. rER: rough ER; Nu:
836 nucleus; cVAC: cytoplasmic viral assembly compartment.
837
838 **FIG 8. STEM tomography of UL148-dependent ER structures in HCMV infected**
839 **cells.** Human fibroblasts infected with wildtype HCMV (TB_WT) were fixed by high-
840 pressure freezing and freeze substitution at day 5 postinfection and tomograms were
841 recorded by STEM. (**A**) Shows a virtual section through the tomogram of a virus-
842 induced membranous structure; asterisks denote ER structures of distended lumenal
843 space. White arrowheads indicate sites at which membranes originating from distended
844 ER cisternae continue into areas of involuted collapsed ER. Scale bar: 1 µm. (**B**)

845 Shows the same virtual section as in (A) tilted and with a 3D visualization of the
846 membranous network (green) of the entire tomogram. The same distended ER
847 cisternae as in (A) are marked by asterisks. (**C**) Shows a cross section through (B) to
848 visualize the membrane profile of the membranous structures. The region delimited by
849 a white box is shown in a higher magnification on the right. Finer detail of the enlarged
850 ER cisternae and the connections between them are readily visible; asterisks indicate
851 the same distended ER cisternae as in (A) and (B). Also, see SI Movie S1. Scale bar: 1
852 µm.
853
854 **FIG 9**. Solubility Analysis of UL148 and Rh159. (A) Human fibroblasts were infected at
855 MOI 1 $TCID_{50}$/cell with HCMV strain TB40/E derived viruses TB_148^{HA}, which
856 expresses UL148 fused at its C-terminus to an HA-epitope tag, or TB_159^{HA}, which
857 lacks *UL148* and instead expresses rhesus CMV Rh159 carrying a C-terminal HA tag.
858 At the indicated times postinfection (hpi), infected cells were collected
859 radioimmunoprecipitation (RIPA) lysis buffer. Lysates were then centrifuged at
860 21,000×g for 30 min, after which supernatant (sup) and pellet (pel) fractions were boiled
861 in gel loading loading buffer containing 2% sodium dodecyl sulfate (SDS). Equivalent
862 portions of supernatant and pellet were then resolved by SDS-polyacrylamide gel
863 electrophoresis, and transferred to a nitrocellulose membrane for detection of protein
864 species immunoreactive to antibodies against HA epitope (HA) and HCMV glycoprotein
865 B (gB) and for total protein signal using Ponceau S reagent (Ponc.). (B-C). Signal
866 intensity of fluorescent conjugated secondary antibodies following anti-HA Western blot
867 was measured and plotted for detergent solubility analysis for experiment shown in (A)

868 or an independent biological replicate in which a 1% NP-40 lysis buffer was used
869 instead of RIPA buffer. Results are shown both as the arbitrary signal (in thousands) or
870 as a ratio of the signal from the pellet: soluble fractions, as indicated.
871
872 **FIG 10. UL148 is sufficient to remodel the ER.** HA-tagged UL148 or Rh159 were
873 doxycycline (dox) induced in the context of a "tet-on" lentiviral vector system in stably
874 transduced ARPE-19 epithelial cell populations, i148^{HA} and i159^{HA}, respectively. Cells
875 were fixed at 48 h postinduction for indirect immunofluorescence staining for the
876 indicated cellular markers (green) together with HA (magenta). Scale bar: 10 µm.
877
878 **FIG 11. ISR activation accompanies redistribution of ER markers during ectopic**
879 **expression of UL148. (A)** Lysates of tet-on ARPE-19 cells expressing either UL148 or
880 Rh159 fused to an HA tag, i148HA and i159HA, respectively, were collected at the
881 indicated times post doxycycline (dox) induction and analyzed by Western blot for the
882 expression of the indicated proteins and for the abundance of eIF2α phosphorylated at
883 Ser51 (P-eIF2α) using a phospho-specific antibody. (**B**) Pearson's correlation
884 coefficient (*r*) values were calculated using NIH ImageJ software estimate the degree of
885 co-localization between UL148 (HA signal) and the indicated cellular markers. A
886 minimum of 30 cells were analyzed per marker. Arithmetic means for each co-
887 localization analysis result are shown as blue lines, and data points for individual cells
888 analyzed are plotted as circles.
889

890 **FIG 12. Live Cell Imaging of UL148-GFP and Rh159-GFP during Induced Ectopic**
891 **Expression.** "Tet-on" ARPE-19 epithelial cells that inducibly express either UL148 or
892 Rh159 fused to green florescent protein (gfp), i148^{gfp} (**A**) and i159^{gfp} (**B**), respectively,
893 were induced for transgene expression using 100 ng/mL doxycycline (dox) and imaged
894 using live-cell microscopy. Images from the selected time points (h post treatment with
895 dox, hpt) are shown. Main scale bar represents 50 μm. For inset panels at upper left of
896 each image, which are magnified 2.4× relative to the main image, the scale bar
897 represents 10 μm. Also see SI Movies S2-S3.
898
899
900 **FIG 13. FRAP analysis.** ARPE-19 cells that inducibly express Rh159-GFP, i159^{gfp} (**A**)
901 or UL148-GFP, i148^{gfp} (**B-C**) were doxycycline induced for 24 h (100 ng/mL doxycycline
902 (dox). Separate regions of GFP signal in selected cells were photobleached (405 nm
903 laser) or left unbleached, while a third region lacking GFP signal was chosen as a
904 background reference were measured before and during fluorescence recovery after
905 photobleaching (FRAP). Note: background signal was not plotted because values were
906 resolvable from the x-axis. GFP signal intensity is plotted over a time period (seconds,
907 s) starting with an exposure at t=0 (immediately before photobleaching), and including
908 measurements taken every 2 s after photobleaching (0-20 s) until termination of the
909 measurement series at t=322 s (300 s of FRAP). (**D-F**) Images from the selected time
910 points (s, seconds) immediately before and after bleaching, and during fluorescence
911 recovery period. Also see SI Movies S4-S6.
912

913 **FIG 14: UL148-GFP is stabilized by inhibition of proteasomal but not lysosomal**
914 **degradation.** "Tet-on" ARPE-19 cells that inducibly express UL148-GFP (i148^{gfp}) were
915 induced for 24 h by the addition of 100 ng/mL doxycycline (dox), after which the dox
916 inducing agent was washed out and medium containing either the proteasome inhibitor
917 epoxomicin (20 μM) or the proton pump inhibitor folimycin (115 nM) was added and
918 samples were harvested for Western blot analysis at the indicated times post treatment
919 (h post treatment, hpt) with folimycin or epoximicin. Also see SI Movie S7.
920
921
922 **FIG 15. Inhibition of the integrated stress response impedes UL148-mediated ER**
923 **remodeling.** "Tet-on" ARPE-19 epithelial cells that inducibly express either UL148 or
924 Rh159 fused to green florescent protein (gfp), i148^{gfp} (**A**) and i159^{gfp} (**B**), respectively,
925 were induced for transgene expression using 100 ng/mL doxycycline (dox) in the
926 presence of absence of either ISRIB (200 nM) or GSK2606414 (1.1 μM) and monitored
927 by Western blot for expression of UL148-GFP over a series of time points (h post
928 treatment with dox, hpt). (**C-E**): Live-cell imaging of UL148-GFP and Rh159-GFP
929 expression patterns in the presence of ISRIB (200 nM), GSK2606414 (1.1 μM), or
930 DMSO vehicle alone. Main scale bar represents 50 μm. For inset panels at upper left of
931 each image, which are magnified 2.4× relative to the main image, the scale bar
932 represents 10 μm. Also see SI Movies S8-S10.
933
934

935 **FIG 16. Inhibition of the ISR prevents the coalescence of Hrd1 and UL148 into**
936 **discrete structures during infection.** (A) Representative 3D maximum intensity
937 projections of confocal imaging Z-stacks obtained from cells infected at MOI 1 for 96 h
938 with HCMV strain TB40/E carrying an HA-tagged *UL148*, TB_148^{HA}, and maintained in
939 the presence of ISRIB (200 nM), GSK2606414 (1.1 μM), or DMSO carrier alone (0.1%
940 vol/vol). In merged images HA signal is shown in magenta, Hrd1 in green, and DAPI
941 counterstaining in blue. (B) The percent of Hrd1 antibody signals that were involved in
942 discrete structures at 96 hpi were calculated for a minimum of 30 cells per condition were
943 determined using Imaris x64 9.3.0 software. Statistical significance was determined using
944 a one-way ANOVA followed by Tukey's post-test; **** represents a P-value of <0.0001.
945 The arithmetic mean for each co-localization analysis result is shown as a blue line, and
946 data points for individual cells analyzed are plotted as circles. (C-D) Western blot
947 analyses of fibroblasts infected at MOI 1 with TB_148^{HA} and maintained in the presence
948 of ISRIB (200 nM), GSK2606414 (1.1 μM), or DMSO carrier alone (0.1%); hpi: h post
949 infection (hpi). Note: a phospho-specific antibody was used for detection of eIF2α
950 phosphorylated at Ser51 (P-eIF2α).
951
952
953
954 **SI FIGURES and MOVIES.**
955
956 **Fig S1**: (A) Lower magnification overview of results from Fig 1A-B; confocal indirect
957 immunofluorescence staining of HCMV glycoprotein H (gH) and Hrd1 at 96 h
958 postinfection of human fibroblasts with wildtype HCMV strain TB40/E (WT) versus
959 *UL148*-null derivative TB_148$_{STOP}$. (B) Confocal indirect immunofluorescence staining

960 of gH and Hrd1 at 96 h postinfection of human fibroblasts with wildtype Merlin recovered
961 from BAC-cloned Merlin pAL1393 (ME_WT) or a *UL148*-null derivative of the same
962 virus (ME_148$_{STOP}$.) (C): Confocal indirect immunofluorescence staining of gH and
963 Hrd1 at 96 h postinfection of human fibroblasts with wildtype HCMV strain TRgfp
964 recovered from BAC-cloned TRgfp (TR_WT) or a *UL148*-null derivative of the same
965 virus (TR_148$_{STOP}$). (D) Confocal indirect immunofluorescence staining of the viral
966 tegument protein UL71 and calnexin at 5 days postinfection of human fibroblasts with
967 primary clinical HCMV isolates obtained from patient throat swabs. (E) Confocal
968 indirect immunofluorescence staining against HA and Hrd1 in THP-1 macrophages fixed
969 at 96 h postinfection with HCMV strain TB40/E derivative viruses TB_148^{HA} or
970 TB_159^{HA}; note: THP-1 monocytes were differentiated using phorbol ester treatment.
971 (**F**) Confocal indirect immunofluorescence staining of HA and Hrd1 in ARPE-19
972 epithelial cells infected for 96 h with either TB_148^{HA} or TB_159^{HA}. (**G**) Confocal indirect
973 immunofluorescence staining of HA and Hrd1 in ARPE-19 epithelial cells infected for 96
974 h with HCMV strain AD169 repaired for *UL131* and to which an HA-tagged UL148 CDS
975 from TB40/E was restored to the native *UL148* locus (AD^{r131}_148^{HA}) or with a parental
976 AD169 virus repaired for *UL131* to which *UL148* was not restored (AD^{r131}). Note: (i) a
977 functional *UL131* is required for efficient infection of epithelial cells; (ii) the difference in
978 scale bar between ADr131 and ADr131_148^{HA} is because with ADr131 we did not have
979 a viral marker (e.g., HA) to identify infected cells, so the appearance of syncytia and the
980 characteristic kidney-bean shaped nucleus was used to indicate infected cells, hence
981 the use of a slightly lower magnification. (**H**) Confocal indirect immunofluorescence

982 staining of telomerase-immortalized rhesus fibroblasts infected with BAC derived rhesus
983 CMV (RhCMV) strain 68-1 carrying an HA-tag at the C-terminus of Rh159.
984
985
986 **FIG S2: Confocal microscopy of LC3B, syntaxin-6 and glycoprotein H staining**
987 **during HCMV infection.** Human fibroblasts were infected with the indicated viruses for
988 96 h and then fixed, permeabilized, and stained using antibodies specific for the
989 indicated proteins. Indirect immunofluorescence images were captured using a 63X
990 objective on a Leica SP5 confocal microscope. gH: glycoprotein H, STX6: syntaxin-6.
991
992
993
994 **MOVIE S1:** TEM tomography of anomalous ER structures in wildtype HCMV infected
995 fibroblasts at day 5 postinfection.
996
997 **MOVIES S2 – S7: Live cell imaging of GFP signal following dox induction of**
998 **transgene expression in i148^{gfp} and i159^{gfp} ARPE-19 epithelial cells.**
999
1000 **Movie S2: i148^{gfp} cells from 2-19 h post dox induction.**
1001 **Movie S3:** i159^{gfp} cells from 2-19 h post dox induction.
1002
1003 **Movie S4**: **FRAP of UL148-GFP structure (ER within structure)**
1004 **Movie S5: FRAP of UL148 GFP structure (ER outside structure)**
1005 **Movie S6: FRAP of Rh159-GFP.**

1006

1007 **Movie S7: Imaging of UL148-GFP following washout of doxycycline.** (to 21 h 37

1008 min post washout).

1009

1010 **Movie S8: i148^{gfp} cells in the presence of 0.1% DMSO, from 2-19 h post dox**

1011 **induction.**

1012 **Movie S9: i148^{gfp} cells in the presence of 1.1 μM GSK2606414, from 2-19 h post**

1013 **dox induction.**

1014 **Movie S10: i148^{gfp} cells in the presence of 200 nM ISRIB, from 2-19 h post dox**

1015 **induction.**

1016

1017
1018

1019

1. Li G, Nguyen CC, Ryckman BJ, Britt WJ, Kamil JP. 2015. A viral regulator of glycoprotein complexes contributes to human cytomegalovirus cell tropism. Proc Natl Acad Sci U S A 112:4471-6.
2. Wille PT, Knoche AJ, Nelson JA, Jarvis MA, Johnson DC. 2010. A human cytomegalovirus gO-null mutant fails to incorporate gH/gL into the virion envelope and is unable to enter fibroblasts and epithelial and endothelial cells. J Virol 84:2585-96.
3. Jiang XJ, Adler B, Sampaio KL, Digel M, Jahn G, Ettischer N, Stierhof YD, Scrivano L, Koszinowski U, Mach M, Sinzger C. 2008. UL74 of human cytomegalovirus contributes to virus release by promoting secondary envelopment of virions. J Virol 82:2802-12.
4. Zhou M, Lanchy JM, Ryckman BJ. 2015. Human Cytomegalovirus gH/gL/gO Promotes the Fusion Step of Entry into All Cell Types, whereas gH/gL/UL128-131 Broadens Virus Tropism through a Distinct Mechanism. J Virol 89:8999-9009.
5. Wu Y, Prager A, Boos S, Resch M, Brizic I, Mach M, Wildner S, Scrivano L, Adler B. 2017. Human cytomegalovirus glycoprotein complex gH/gL/gO uses PDGFR-alpha as a key for entry. PLoS Pathog 13:e1006281.
6. Kabanova A, Marcandalli J, Zhou T, Bianchi S, Baxa U, Tsybovsky Y, Lilleri D, Silacci-Fregni C, Foglierini M, Fernandez-Rodriguez BM, Druz A, Zhang B, Geiger R, Pagani M, Sallusto F, Kwong PD, Corti D, Lanzavecchia A, Perez L. 2016. Platelet-derived growth factor-alpha receptor is the cellular receptor for human cytomegalovirus gHgLgO trimer. Nat Microbiol 1:16082.
7. Wu K, Oberstein A, Wang W, Shenk T. 2018. Role of PDGF receptor-alpha during human cytomegalovirus entry into fibroblasts. Proc Natl Acad Sci U S A doi:10.1073/pnas.1806305115.
8. Nguyen CC, Siddiquey MNA, Zhang H, Li G, Kamil JP. 2018. Human Cytomegalovirus Tropism Modulator UL148 Interacts with SEL1L, a Cellular Factor That Governs Endoplasmic Reticulum-Associated Degradation of the Viral Envelope Glycoprotein gO. J Virol 92:e00688-18.
9. Wang ECY, Pjechova M, Nightingale K, Vlahava VM, Patel M, Ruckova E, Forbes SK, Nobre L, Antrobus R, Roberts D, Fielding CA, Seirafian S, Davies J, Murrell I, Lau B, Wilkie GS, Suarez NM, Stanton RJ, Vojtesek B, Davison A, Lehner PJ, Weekes MP, Wilkinson GWG, Tomasec P. 2018. Suppression of costimulation by human cytomegalovirus promotes evasion of cellular immune defenses. Proc Natl Acad Sci U S A 115:4998-5003.
10. Siddiquey MNA, Zhang H, Nguyen CC, Domma AJ, Kamil JP. 2018. The Human Cytomegalovirus Endoplasmic Reticulum-Resident Glycoprotein UL148 Activates the Unfolded Protein Response. J Virol 92:e00896-18.
11. Das S, Vasanji A, Pellett PE. 2007. Three-dimensional structure of the human cytomegalovirus cytoplasmic virion assembly complex includes a reoriented secretory apparatus. J Virol 81:11861-9.

1061 12. Sanchez V, Greis KD, Sztul E, Britt WJ. 2000. Accumulation of virion tegument and
1062 envelope proteins in a stable cytoplasmic compartment during human cytomegalovirus
1063 replication: characterization of a potential site of virus assembly. J Virol 74:975-86.
1064 13. Lilley BN, Ploegh HL. 2005. Multiprotein complexes that link dislocation, ubiquitination,
1065 and extraction of misfolded proteins from the endoplasmic reticulum membrane. Proc
1066 Natl Acad Sci U S A 102:14296-301.
1067 14. Kamhi-Nesher S, Shenkman M, Tolchinsky S, Fromm SV, Ehrlich R, Lederkremer GZ.
1068 2001. A novel quality control compartment derived from the endoplasmic reticulum.
1069 Mol Biol Cell 12:1711-23.
1070 15. Leitman J, Shenkman M, Gofman Y, Shtern NO, Ben-Tal N, Hendershot LM, Lederkremer
1071 GZ. 2014. Herp coordinates compartmentalization and recruitment of HRD1 and
1072 misfolded proteins for ERAD. Mol Biol Cell 25:1050-60.
1073 16. Houck SA, Ren HY, Madden VJ, Bonner JN, Conlin MP, Janovick JA, Conn PM, Cyr DM.
1074 2014. Quality control autophagy degrades soluble ERAD-resistant conformers of the
1075 misfolded membrane protein GnRHR. Mol Cell 54:166-179.
1076 17. Sturgill ER, Malouli D, Hansen SG, Burwitz BJ, Seo S, Schneider CL, Womack JL, Verweij
1077 MC, Ventura AB, Bhusari A, Jeffries KM, Legasse AW, Axthelm MK, Hudson AW, Sacha
1078 JB, Picker LJ, Fruh K. 2016. Natural Killer Cell Evasion Is Essential for Infection by Rhesus
1079 Cytomegalovirus. PLoS Pathog 12:e1005868.
1080 18. Chaumorcel M, Souquere S, Pierron G, Codogno P, Esclatine A. 2008. Human
1081 cytomegalovirus controls a new autophagy-dependent cellular antiviral defense
1082 mechanism. Autophagy 4:46-53.
1083 19. Chaumorcel M, Lussignol M, Mouna L, Cavignac Y, Fahie K, Cotte-Laffitte J, Geballe A,
1084 Brune W, Beau I, Codogno P, Esclatine A. 2012. The human cytomegalovirus protein
1085 TRS1 inhibits autophagy via its interaction with Beclin 1. J Virol 86:2571-84.
1086 20. Alwine JC. 2012. The human cytomegalovirus assembly compartment: a masterpiece of
1087 viral manipulation of cellular processes that facilitates assembly and egress. PLoS Pathog
1088 8:e1002878.
1089 21. Das S, Pellett PE. 2011. Spatial relationships between markers for secretory and
1090 endosomal machinery in human cytomegalovirus-infected cells versus those in
1091 uninfected cells. J Virol 85:5864-79.
1092 22. Leitman J, Ron E, Ogen-Shtern N, Lederkremer GZ. 2013. Compartmentalization of
1093 endoplasmic reticulum quality control and ER-associated degradation factors. DNA Cell
1094 Biol 32:2-7.
1095 23. Cox DW, Billingsley GD, Callahan JW. 1986. Aggregation of plasma Z type alpha 1-
1096 antitrypsin suggests basic defect for the deficiency. FEBS Lett 205:255-60.
1097 24. Le A, Ferrell GA, Dishon DS, Le QQ, Sifers RN. 1992. Soluble aggregates of the human PiZ
1098 alpha 1-antitrypsin variant are degraded within the endoplasmic reticulum by a
1099 mechanism sensitive to inhibitors of protein synthesis. J Biol Chem 267:1072-80.
1100 25. Lomas DA, Evans DL, Finch JT, Carrell RW. 1992. The mechanism of Z alpha 1-antitrypsin
1101 accumulation in the liver. Nature 357:605-7.
1102 26. Ordonez A, Snapp EL, Tan L, Miranda E, Marciniak SJ, Lomas DA. 2013. Endoplasmic
1103 reticulum polymers impair luminal protein mobility and sensitize to cellular stress in
1104 alpha1-antitrypsin deficiency. Hepatology 57:2049-60.

1105 27. Suhy DA, Giddings TH, Jr., Kirkegaard K. 2000. Remodeling the endoplasmic reticulum by
1106 poliovirus infection and by individual viral proteins: an autophagy-like origin for virus-
1107 induced vesicles. J Virol 74:8953-65.
1108 28. Windsor M, Hawes P, Monaghan P, Snapp E, Salas ML, Rodriguez JM, Wileman T. 2012.
1109 Mechanism of collapse of endoplasmic reticulum cisternae during African swine fever
1110 virus infection. Traffic 13:30-42.
1111 29. Miller S, Krijnse-Locker J. 2008. Modification of intracellular membrane structures for
1112 virus replication. Nat Rev Microbiol 6:363-74.
1113 30. Siddiquey MNA, Zhang H, Nguyen CC, Domma AJ, Kamil JP. 2018. The human
1114 cytomegalovirus ER resident glycoprotein UL148 activates the unfolded protein
1115 response. J Virol doi:10.1128/JVI.00896-18.
1116 31. Cormack BP, Valdivia RH, Falkow S. 1996. FACS-optimized mutants of the green
1117 fluorescent protein (GFP). Gene 173:33-8.
1118 32. Khaminets A, Heinrich T, Mari M, Grumati P, Huebner AK, Akutsu M, Liebmann L, Stolz
1119 A, Nietzsche S, Koch N, Mauthe M, Katona I, Qualmann B, Weis J, Reggiori F, Kurth I,
1120 Hubner CA, Dikic I. 2015. Regulation of endoplasmic reticulum turnover by selective
1121 autophagy. Nature 522:354-8.
1122 33. Meng L, Mohan R, Kwok BH, Elofsson M, Sin N, Crews CM. 1999. Epoxomicin, a potent
1123 and selective proteasome inhibitor, exhibits in vivo antiinflammatory activity. Proc Natl
1124 Acad Sci U S A 96:10403-8.
1125 34. Muroi M, Shiragami N, Nagao K, Yamasaki M, Takatsuki A. 1993. Folimycin
1126 (concanamycin A), a specific inhibitor of V-ATPase, blocks intracellular translocation of
1127 the glycoprotein of vesicular stomatitis virus before arrival to the Golgi apparatus. Cell
1128 Struct Funct 18:139-49.
1129 35. Muroi M, Takasu A, Yamasaki M, Takatsuki A. 1993. Folimycin (concanamycin A), an
1130 inhibitor of V-type H(+)-ATPase, blocks cell-surface expression of virus-envelope
1131 glycoproteins. Biochem Biophys Res Commun 193:999-1005.
1132 36. Kondratyev M, Avezov E, Shenkman M, Groisman B, Lederkremer GZ. 2007. PERK-
1133 dependent compartmentalization of ERAD and unfolded protein response machineries
1134 during ER stress. Exp Cell Res 313:3395-407.
1135 37. Harding HP, Novoa I, Zhang Y, Zeng H, Wek R, Schapira M, Ron D. 2000. Regulated
1136 translation initiation controls stress-induced gene expression in mammalian cells. Mol
1137 Cell 6:1099-108.
1138 38. Palam LR, Baird TD, Wek RC. 2011. Phosphorylation of eIF2 facilitates ribosomal bypass
1139 of an inhibitory upstream ORF to enhance CHOP translation. J Biol Chem 286:10939-49.
1140 39. Vattem KM, Wek RC. 2004. Reinitiation involving upstream ORFs regulates ATF4 mRNA
1141 translation in mammalian cells. Proc Natl Acad Sci U S A 101:11269-74.
1142 40. Sidrauski C, Acosta-Alvear D, Khoutorsky A, Vedantham P, Hearn BR, Li H, Gamache K,
1143 Gallagher CM, Ang KK, Wilson C, Okreglak V, Ashkenazi A, Hann B, Nader K, Arkin MR,
1144 Renslo AR, Sonenberg N, Walter P. 2013. Pharmacological brake-release of mRNA
1145 translation enhances cognitive memory. Elife 2:e00498.
1146 41. Sidrauski C, McGeachy AM, Ingolia NT, Walter P. 2015. The small molecule ISRIB
1147 reverses the effects of eIF2alpha phosphorylation on translation and stress granule
1148 assembly. Elife 4.

1149 42. Zyryanova AF, Weis F, Faille A, Alard AA, Crespillo-Casado A, Sekine Y, Harding HP, Allen
1150 F, Parts L, Fromont C, Fischer PM, Warren AJ, Ron D. 2018. Binding of ISRIB reveals a
1151 regulatory site in the nucleotide exchange factor eIF2B. Science 359:1533-1536.
1152 43. Sidrauski C, Tsai JC, Kampmann M, Hearn BR, Vedantham P, Jaishankar P, Sokabe M,
1153 Mendez AS, Newton BW, Tang EL, Verschueren E, Johnson JR, Krogan NJ, Fraser CS,
1154 Weissman JS, Renslo AR, Walter P. 2015. Pharmacological dimerization and activation of
1155 the exchange factor eIF2B antagonizes the integrated stress response. Elife 4:e07314.
1156 44. Tsai JC, Miller-Vedam LE, Anand AA, Jaishankar P, Nguyen HC, Renslo AR, Frost A, Walter
1157 P. 2018. Structure of the nucleotide exchange factor eIF2B reveals mechanism of
1158 memory-enhancing molecule. Science 359.
1159 45. Gordiyenko Y, Schmidt C, Jennings MD, Matak-Vinkovic D, Pavitt GD, Robinson CV. 2014.
1160 eIF2B is a decameric guanine nucleotide exchange factor with a gamma2epsilon2
1161 tetrameric core. Nat Commun 5:3902.
1162 46. Harding HP, Zhang Y, Ron D. 1999. Protein translation and folding are coupled by an
1163 endoplasmic-reticulum-resident kinase. Nature 397:271-4.
1164 47. Harding HP, Zhang Y, Bertolotti A, Zeng H, Ron D. 2000. Perk is essential for translational
1165 regulation and cell survival during the unfolded protein response. Mol Cell 5:897-904.
1166 48. Axten JM, Medina JR, Feng Y, Shu A, Romeril SP, Grant SW, Li WH, Heerding DA,
1167 Minthorn E, Mencken T, Atkins C, Liu Q, Rabindran S, Kumar R, Hong X, Goetz A, Stanley
1168 T, Taylor JD, Sigethy SD, Tomberlin GH, Hassell AM, Kahler KM, Shewchuk LM, Gampe
1169 RT. 2012. Discovery of 7-methyl-5-(1-{[3-(trifluoromethyl)phenyl]acetyl}-2,3-dihydro-1H-
1170 indol-5-yl)-7H-p yrrolo[2,3-d]pyrimidin-4-amine (GSK2606414), a potent and selective
1171 first-in-class inhibitor of protein kinase R (PKR)-like endoplasmic reticulum kinase
1172 (PERK). J Med Chem 55:7193-207.
1173 49. Tenorio R, Fernandez de Castro I, Knowlton JJ, Zamora PF, Lee CH, Mainou BA, Dermody
1174 TS, Risco C. 2018. Reovirus sigmaNS and muNS Proteins Remodel the Endoplasmic
1175 Reticulum to Build Replication Neo-Organelles. MBio 9.
1176 50. Miller S, Kastner S, Krijnse-Locker J, Buhler S, Bartenschlager R. 2007. The non-structural
1177 protein 4A of dengue virus is an integral membrane protein inducing membrane
1178 alterations in a 2K-regulated manner. J Biol Chem 282:8873-82.
1179 51. Lamond AI, Sleeman JE. 2003. Nuclear substructure and dynamics. Curr Biol 13:R825-8.
1180 52. Granell S, Baldini G, Mohammad S, Nicolin V, Narducci P, Storrie B, Baldini G. 2008.
1181 Sequestration of mutated alpha1-antitrypsin into inclusion bodies is a cell-protective
1182 mechanism to maintain endoplasmic reticulum function. Mol Biol Cell 19:572-86.
1183 53. Lawless MW, Greene CM, Mulgrew A, Taggart CC, O'Neill SJ, McElvaney NG. 2004.
1184 Activation of endoplasmic reticulum-specific stress responses associated with the
1185 conformational disease Z alpha 1-antitrypsin deficiency. J Immunol 172:5722-6.
1186 54. Tirosh B, Iwakoshi NN, Lilley BN, Lee AH, Glimcher LH, Ploegh HL. 2005. Human
1187 cytomegalovirus protein US11 provokes an unfolded protein response that may
1188 facilitate the degradation of class I major histocompatibility complex products. J Virol
1189 79:2768-79.
1190 55. Wiertz EJ, Jones TR, Sun L, Bogyo M, Geuze HJ, Ploegh HL. 1996. The human
1191 cytomegalovirus US11 gene product dislocates MHC class I heavy chains from the
1192 endoplasmic reticulum to the cytosol. Cell 84:769-79.

1193 56. van den Boomen DJ, Timms RT, Grice GL, Stagg HR, Skodt K, Dougan G, Nathan JA,
1194 Lehner PJ. 2014. TMEM129 is a Derlin-1 associated ERAD E3 ligase essential for virus-
1195 induced degradation of MHC-I. Proc Natl Acad Sci U S A 111:11425-30.
1196 57. Caramelo JJ, Parodi AJ. 2008. Getting in and out from calnexin/calreticulin cycles. J Biol
1197 Chem 283:10221-5.
1198 58. Hammond C, Braakman I, Helenius A. 1994. Role of N-linked oligosaccharide
1199 recognition, glucose trimming, and calnexin in glycoprotein folding and quality control.
1200 Proc Natl Acad Sci U S A 91:913-7.
1201 59. Zhou M, Yu Q, Wechsler A, Ryckman BJ. 2013. Comparative analysis of gO isoforms
1202 reveals that strains of human cytomegalovirus differ in the ratio of gH/gL/gO and
1203 gH/gL/UL128-131 in the virion envelope. J Virol 87:9680-90.
1204 60. Zhang L, Zhou M, Stanton R, Kamil J, Ryckman BJ. 2018. Expression Levels of
1205 Glycoprotein O (gO) Vary between Strains of Human Cytomegalovirus, Influencing the
1206 Assembly of gH/gL Complexes and Virion Infectivity. J Virol 92.
1207 61. Johnston JA, Ward CL, Kopito RR. 1998. Aggresomes: a cellular response to misfolded
1208 proteins. J Cell Biol 143:1883-98.
1209 62. Johnston JA, Illing ME, Kopito RR. 2002. Cytoplasmic dynein/dynactin mediates the
1210 assembly of aggresomes. Cell Motil Cytoskeleton 53:26-38.
1211 63. Pankiv S, Alemu EA, Brech A, Bruun JA, Lamark T, Overvatn A, Bjorkoy G, Johansen T.
1212 2010. FYCO1 is a Rab7 effector that binds to LC3 and PI3P to mediate microtubule plus
1213 end-directed vesicle transport. J Cell Biol 188:253-69.
1214 64. Hummel T, Krukkert K, Roos J, Davis G, Klambt C. 2000. Drosophila Futsch/22C10 is a
1215 MAP1B-like protein required for dendritic and axonal development. Neuron 26:357-70.
1216 65. Wang H, Bedford FK, Brandon NJ, Moss SJ, Olsen RW. 1999. GABA(A)-receptor-
1217 associated protein links GABA(A) receptors and the cytoskeleton. Nature 397:69-72.
1218 66. Kirchoff V, Wong S, St JS, Pari GS. 2002. Generation of a life-expanded rhesus monkey
1219 fibroblast cell line for the growth of rhesus rhadinovirus (RRV). Arch Virol 147:321-33.
1220 67. Sinzger C, Hahn G, Digel M, Katona R, Sampaio KL, Messerle M, Hengel H, Koszinowski U,
1221 Brune W, Adler B. 2008. Cloning and sequencing of a highly productive, endotheliotropic
1222 virus strain derived from human cytomegalovirus TB40/E. J Gen Virol 89:359-68.
1223 68. Smith IL, Taskintuna I, Rahhal FM, Powell HC, Ai E, Mueller AJ, Spector SA, Freeman WR.
1224 1998. Clinical failure of CMV retinitis with intravitreal cidofovir is associated with
1225 antiviral resistance. Arch Ophthalmol 116:178-85.
1226 69. Murphy E, Yu D, Grimwood J, Schmutz J, Dickson M, Jarvis MA, Hahn G, Nelson JA,
1227 Myers RM, Shenk TE. 2003. Coding potential of laboratory and clinical strains of human
1228 cytomegalovirus. Proc Natl Acad Sci U S A 100:14976-81.
1229 70. Stanton RJ, Baluchova K, Dargan DJ, Cunningham C, Sheehy O, Seirafian S, McSharry BP,
1230 Neale ML, Davies JA, Tomasec P, Davison AJ, Wilkinson GW. 2010. Reconstruction of the
1231 complete human cytomegalovirus genome in a BAC reveals RL13 to be a potent inhibitor
1232 of replication. J Clin Invest 120:3191-208.
1233 71. Chang WL, Barry PA. 2003. Cloning of the full-length rhesus cytomegalovirus genome as
1234 an infectious and self-excisable bacterial artificial chromosome for analysis of viral
1235 pathogenesis. J Virol 77:5073-83.

1236 72. Tischer BK, Smith GA, Osterrieder N. 2010. En passant mutagenesis: a two step
1237 markerless red recombination system. Methods Mol Biol 634:421-30.
1238 73. Tischer BK, von Einem J, Kaufer B, Osterrieder N. 2006. Two-step red-mediated
1239 recombination for versatile high-efficiency markerless DNA manipulation in Escherichia
1240 coli. Biotechniques 40:191-7.
1241 74. Dietz AN, Villinger C, Becker S, Frick M, von Einem J. 2018. A Tyrosine-Based Trafficking
1242 Motif of the Tegument Protein pUL71 Is Crucial for Human Cytomegalovirus Secondary
1243 Envelopment. J Virol 92.
1244 75. Hohn K, Sailer M, Wang L, Lorenz M, Schneider ME, Walther P. 2011. Preparation of
1245 cryofixed cells for improved 3D ultrastructure with scanning transmission electron
1246 tomography. Histochem Cell Biol 135:1-9.
1247 76. Villinger C, Schauflinger M, Gregorius H, Kranz C, Hohn K, Nafeey S, Walther P. 2014.
1248 Three-dimensional imaging of adherent cells using FIB/SEM and STEM. Methods Mol
1249 Biol 1117:617-38.
1250 77. Kremer JR, Mastronarde DN, McIntosh JR. 1996. Computer visualization of three-
1251 dimensional image data using IMOD. J Struct Biol 116:71-6.
1252 78. Britt WJ, Jarvis MA, Drummond DD, Mach M. 2005. Antigenic domain 1 is required for
1253 oligomerization of human cytomegalovirus glycoprotein B. J Virol 79:4066-79.
1254

1255

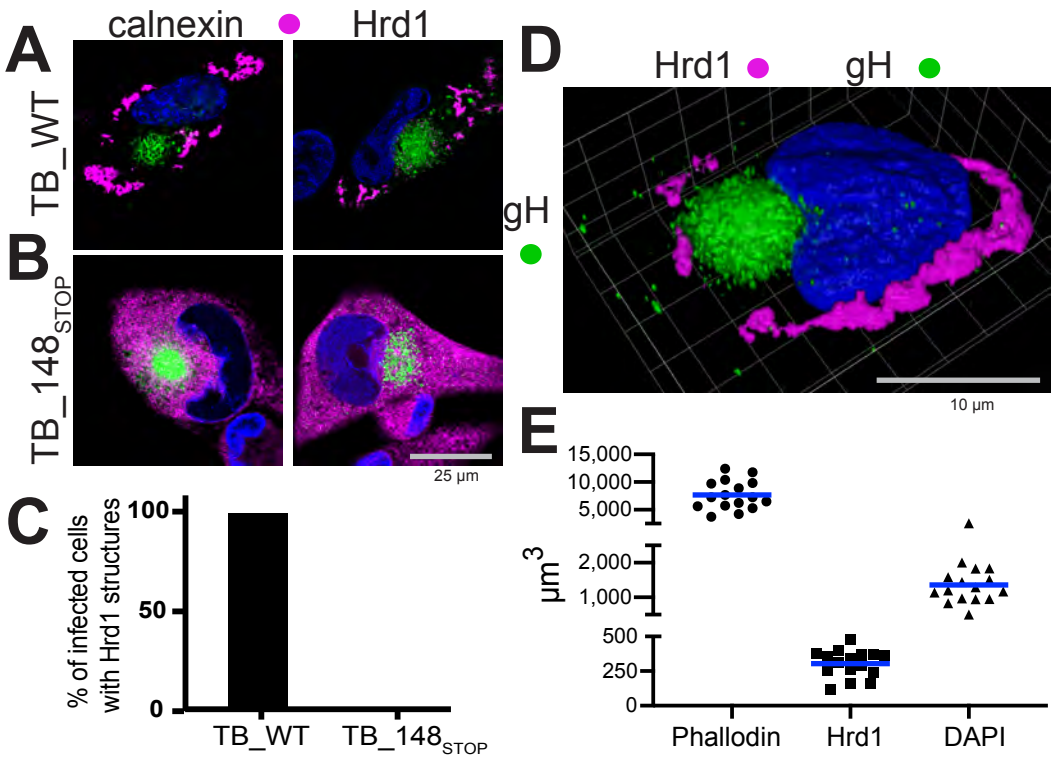

FIG 1. UL148 reorganizes ER markers into anomalous structures during HCMV infection. Fibroblasts infected at 1 MOI with either **(A)** wildtype HCMV strain TB40/E (TB_WT) or **(B)** an isogenic *UL148*-null mutant (TB_148$_{STOP}$), were fixed at 96 h postinfection (hpi) and imaged by confocal microscopy after staining with antibodies specific for CNX or Hrd1 (magenta) and glycoprotein H (gH, green), as indicated. DAPI (blue) signal was used to counterstain nuclei. **(C)** Percentage of fibroblasts that contain Hrd1 structures at 96 hpi, Fifty gH-positive cells for each condition were scored for presence or absence of UL148 structures (also see SI Fig S1A). (**D**) Three-dimensional confocal image projection of a TB_WT infected fibroblast stained at 96 hpi for Hrd1 and gH. **(E)** Volumetric measurements were made from sixteen infected cells, stained with phalloidin-AlexaFluor 594 conjugate to estimate total cell volume, with Hrd1 antibody to estimate the volume of UL148-dependent ER structures, and with DAPI to estimate nuclear volume.

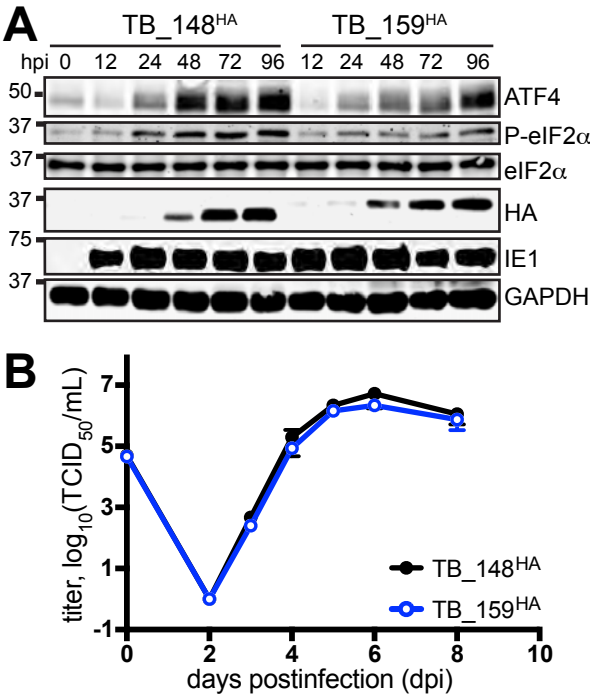

FIG 2. Characterization of TB_148^{HA} and TB_159^{HA} viruses. (A) Human fibroblasts were infected at MOI 1 with the indicated recombinant HCMVs and whole cell lysate samples harvested at the indicated times post-infection (h post-infection: hpi) were analyzed by Western blot to detect HA-tagged UL148 or Rh159, the 72 kD viral nuclear antigen IE1-72 (IE1), and GAPDH. **(B)** Single-cycle viral replication kinetic curves from MOI 1 infected fibroblasts were plotted by determining the titer in tissue culture infectious dose 50 ($TCID_{50}$) from supernatants collected at the indicated times postinfection.

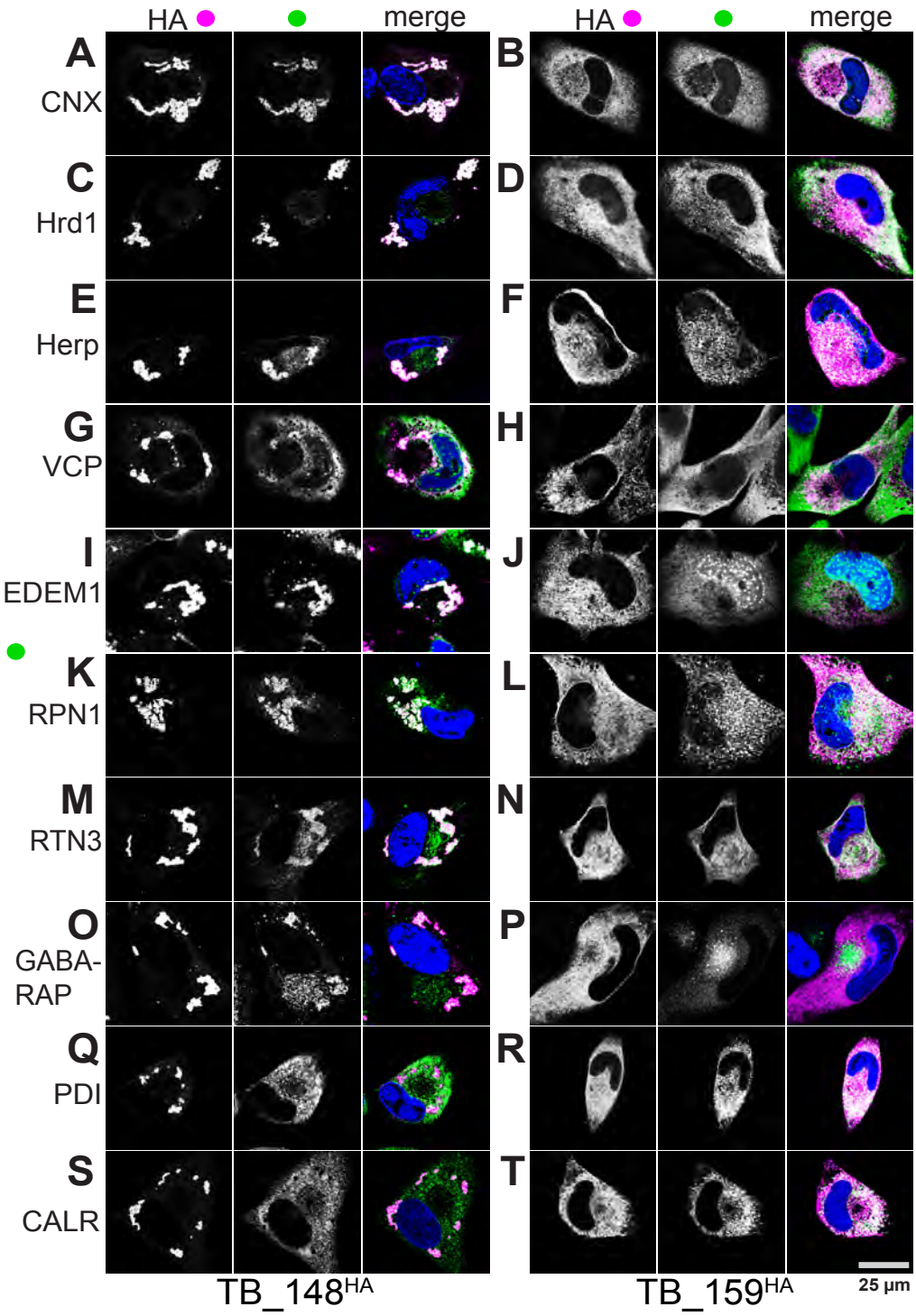

FIG 3. UL148 localizes to unusual ER compartments enriched for glycoprotein quality control markers. Fibroblasts infected at MOI 1 with either TB_148^{HA} (panels: **A, C, E, G, I, K, M, O, Q, S**) or TB_ 159^{HA} (panels: **B, D, F, H, J, L, N, P, R, T**) were fixed at 96 hpi, and imaged by confocal microscopy after co-staining with antibodies specific for HA (UL148/Rh159, magenta in merge) and the indicated cellular markers (green in merge). DAPI (blue) counterstaining is shown in merged image.

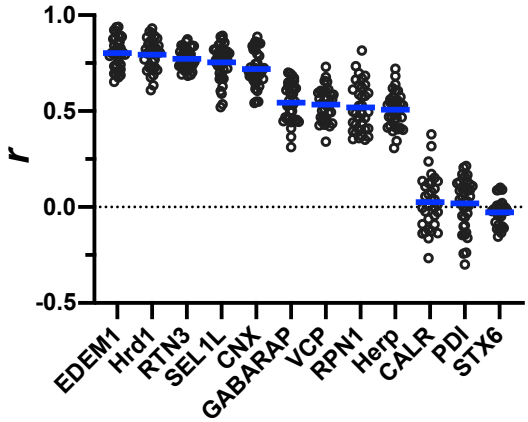

FIG 4. Quantification of Co-localization between UL148 and Cellular Markers. A Pearson's correlation coefficient (*r*) was calculated using NIH ImageJ software to estimate the degree of co-localization between UL148 (HA signal) and each of the indicated cellular markers. A minimum of 30 cells were analyzed per marker. The arithmetic mean for each co-localization analysis result is shown as a blue line, and data points for individual cells analyzed are plotted as circles.

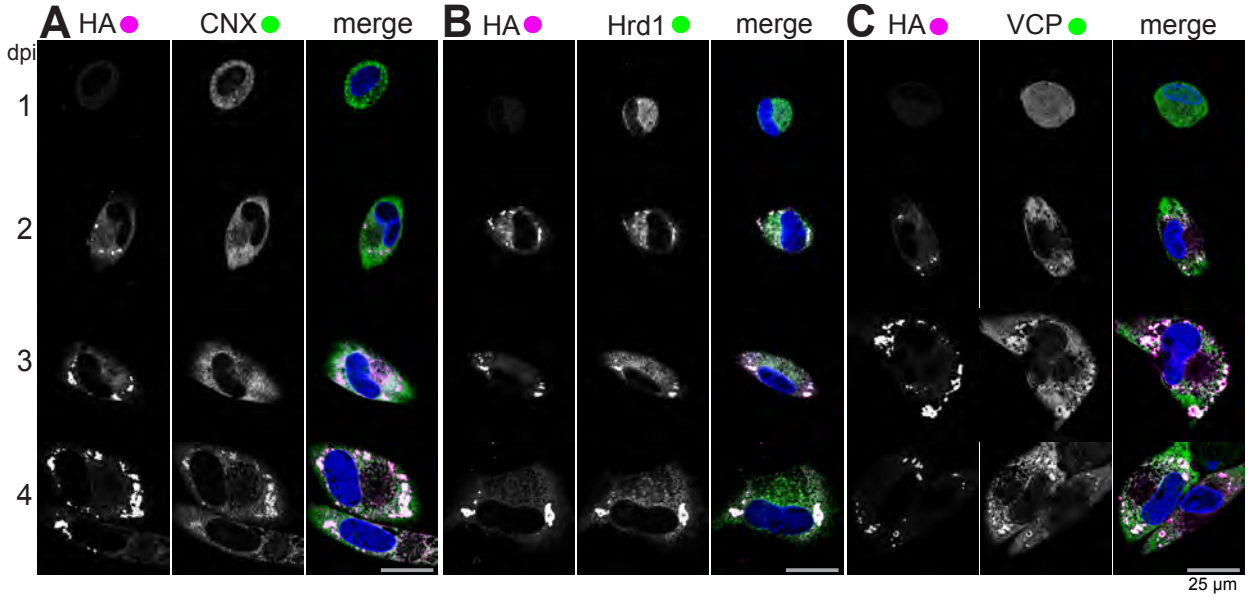

FIG 5. Cellular proteins involved in glycoprotein quality control are recruited with differing kinetics to UL148 ER structures. Fibroblasts infected with TB_148^{HA} at 1 MOI were fixed at the indicated time points (days post infection, dpi) and imaged by confocal microscopy after staining with antibodies specific for HA (UL148, magenta), CNX (green, **A**) , Hrd1 (green, **B**) or VCP(green, **C**), DAPI (blue).

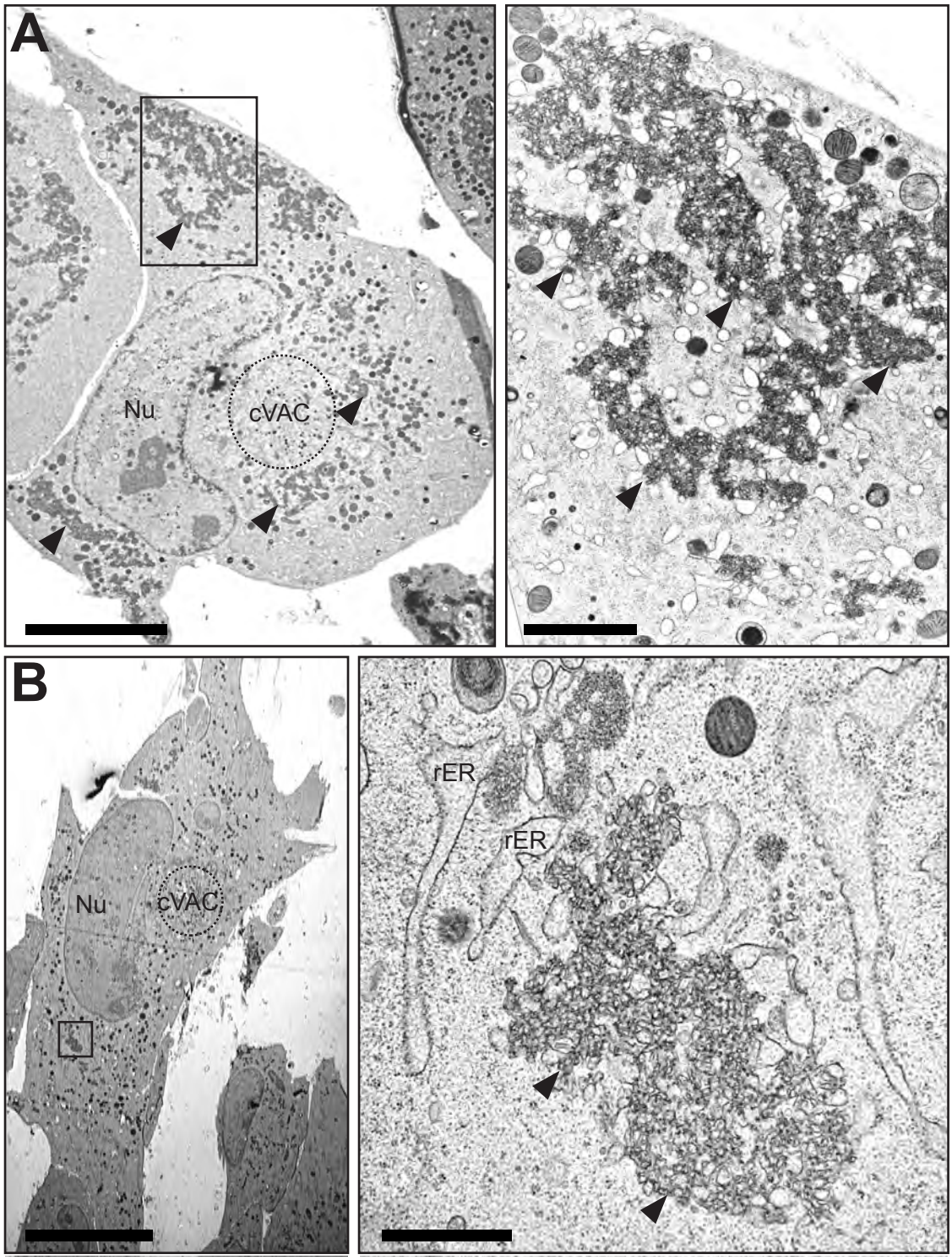

FIG 6. TEM of ER structures in wild-type HCMV infected cells. Human fibroblasts infected with wildtype HCMV (TB_WT) were fixed by high-pressure freezing and freeze substitution at day 5 postinfection and imaged using TEM. Panels (**A**) and (**B**) show cell overview at left. For each cell, the boxed region is shown at higher magnification. Scale bars; left panels: 10 µm, right panels: 2 µm. rER: rough ER; Nu: nucleus; cVAC: cytoplasmic viral assembly compartment. Solid arrowheads indicate the UL148-dependent ER structures of interest.

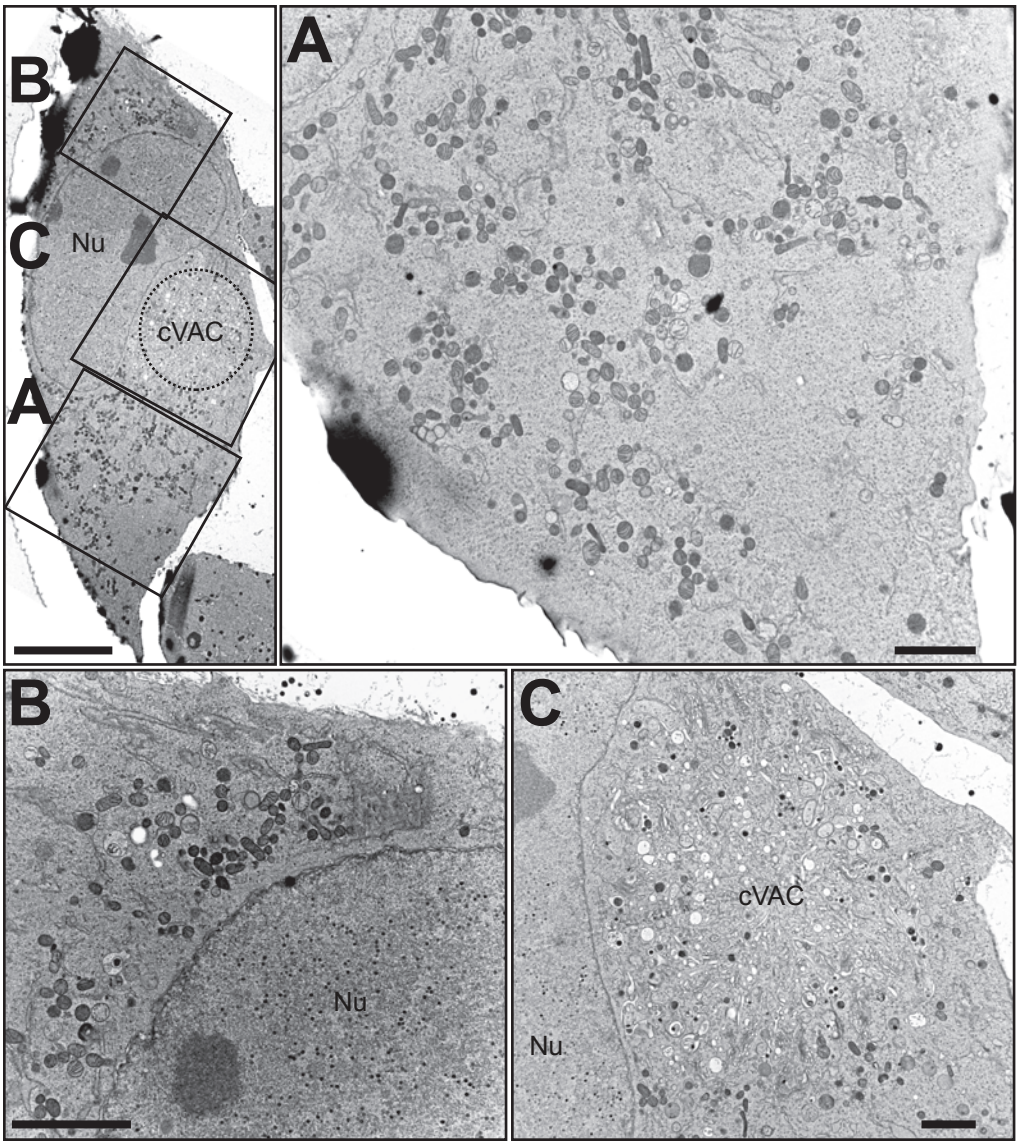

FIG 7. TEM of *UL148*-null HCMV infected cells. Human fibroblasts infected with a *UL148*-null mutant (TB_148$_{STOP}$) were fixed by high-pressure freezing and freeze substitution at day 5 postinfection and imaged using TEM. At the upper left an overview panel of a representative cell is shown with panels **A, B, and C** each boxed. The boxed regions are expanded at higher magnification at right (**A**) and below (**B, C**). Scale bars for upper left overview panel: 10 µm, for zoomed panels: 2 µm. rER: rough ER; Nu: nucleus; cVAC: cytoplasmic viral assembly compartment.

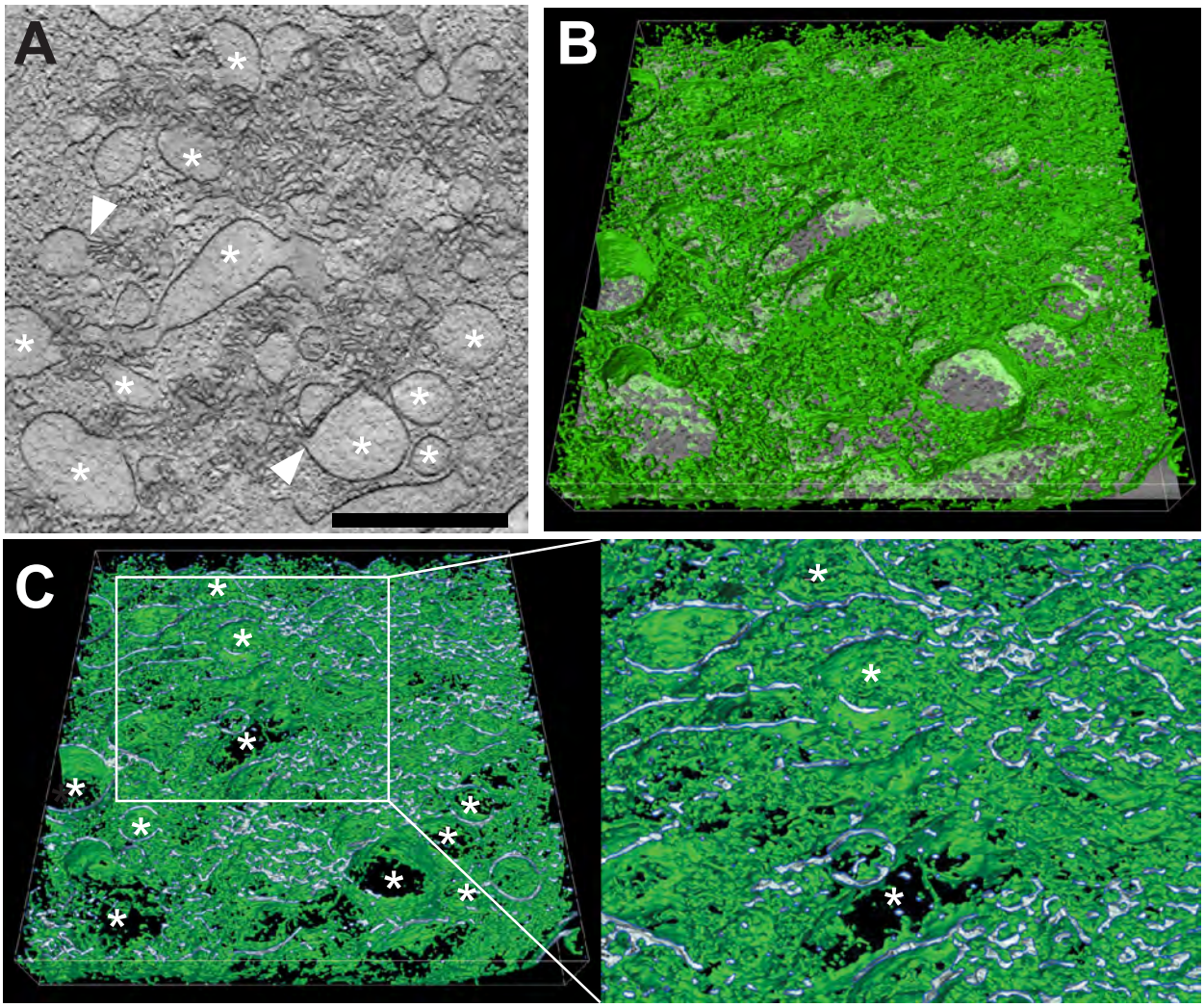

FIG 8. STEM tomography of UL148-dependent ER structures in HCMV infected cells. Human fibroblasts infected with wildtype HCMV (TB_WT) were fixed by high-pressure freezing and freeze substitution at day 5 postinfection and tomograms were recorded by STEM. (**A**) Shows a virtual section through the tomogram of a virus-induced membranous structure; asterisks denote ER structures of distended lumenal space. White arrowheads indicate sites at which membranes originating from distended ER cisternae continue into areas of involuted collapsed ER. Scale bar: 1 µm. (**B**) Shows the same virtual section as in (A) tilted and with a 3D visualization of the membranous network (green) of the entire tomogram. The same distended ER cisternae as in (A) are marked by asterisks. (**C**) Shows a cross section through (B) to visualize the membrane profile of the membranous structures. The region delimited by a white box is shown in a higher magnification on the right. Finer detail of the enlarged ER cisternae and the connections between them are readily visible; asterisks indicate the same distended ER cisternae as in (A) and (B). Also, see SI Movie S1. Scale bar: 1 µm.

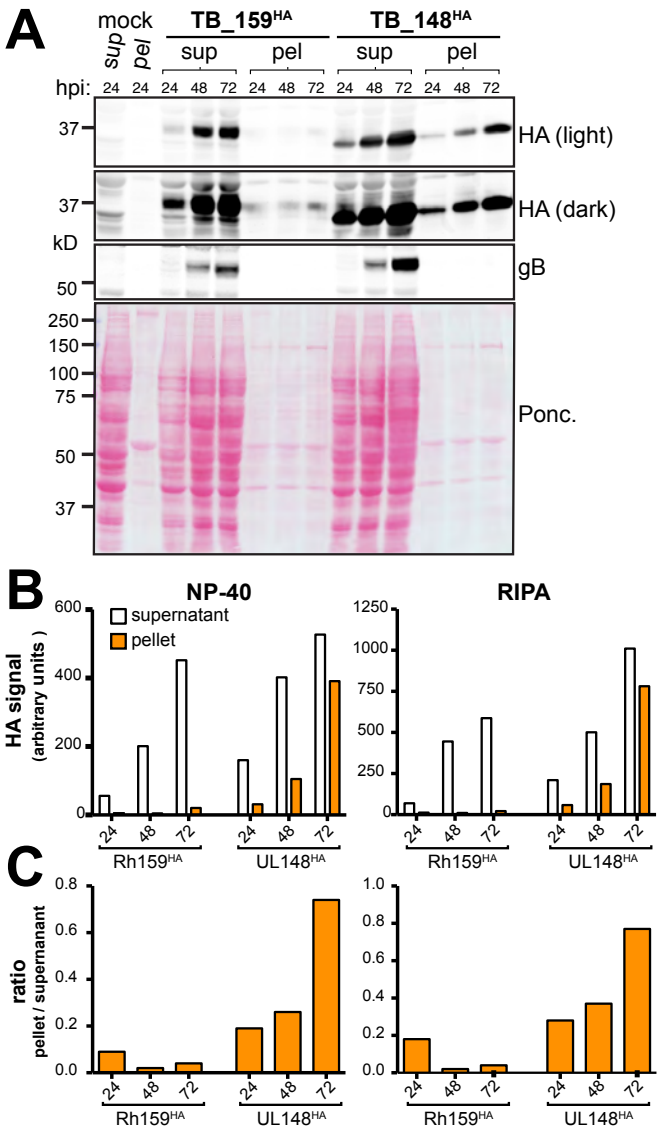

FIG 9. Solubility Analysis of UL148 and Rh159. (A) Human fibroblasts were infected at MOI 1 $TCID_{50}$/cell with HCMV strain TB40/E derived viruses TB_148^{HA}, which expresses UL148 fused at its C-terminus to an HA-epitope tag, or TB_159^{HA}, which lacks *UL148* and instead expresses rhesus CMV Rh159 carrying a C-terminal HA tag. At the indicated times postinfection (hpi), infected cells were collected radioimmunoprecipitation (RIPA) lysis buffer. Lysates were centrifuged at 21,000×g for 30 min, after which supernatant (sup) and pellet (pel) fractions were boiled in gel loading loading buffer containing 2% sodium dodecyl sulfate (SDS). Equivalent portions of supernatant and pellet were then resolved by SDS-polyacrylamide gel electrophoresis, and transferred to a nitrocellulose membrane for detection of protein species immunoreactive to antibodies against HA epitope (HA) and HCMV glycoprotein B (gB) and for total protein signal using Ponceau S reagent (Ponc.). (B-C). Signal intensity of fluorescent conjugated secondary antibodies following anti-HA Western blot was measured and plotted for detergent solubility analysis for experiment shown in (A) or an independent biological replicate in which a 1% NP-40 lysis buffer was used instead of RIPA buffer. Results are shown both as the arbitrary signal (in thousands) or as a ratio of the signal from the pellet: soluble fractions, as indicated.

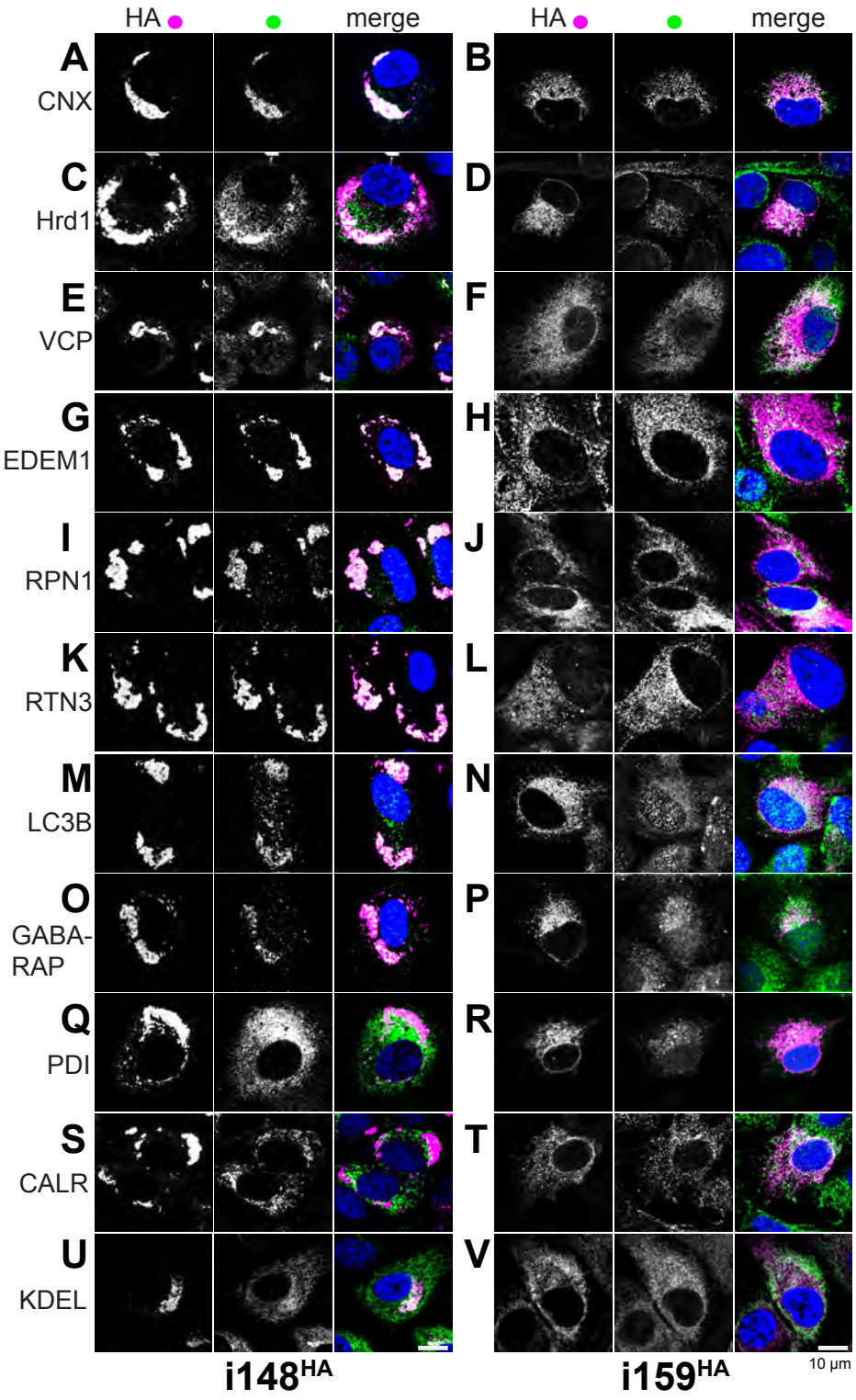

FIG 10. UL148 is sufficient to remodel the ER. HA-tagged UL148 or Rh159 were doxycycline (dox) induced in the context of a "tet-on" lentiviral vector system in stably transduced ARPE-19 epithelial cell populations, i148^{HA} and i159^{HA}, respectively. Cells were fixed at 48 h postinduction for indirect immunofluorescence staining for the indicated cellular markers (green) together with HA (magenta). Scale bar: 10 µm.

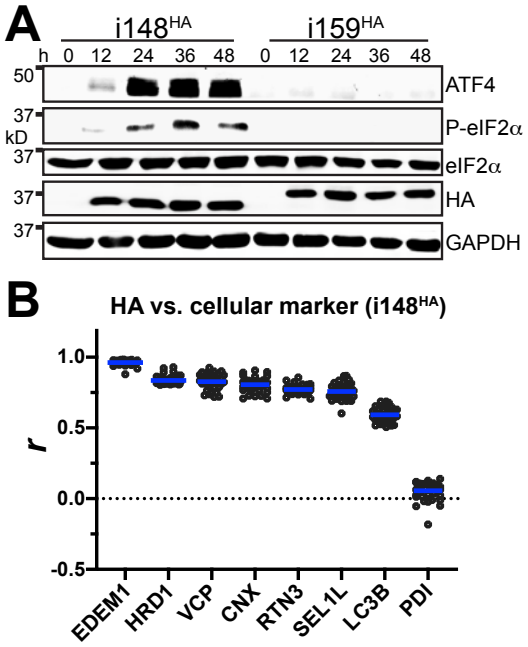

FIG 11. ISR activation accompanies redistribution of ER markers during ectopic expression of UL148. (A) Lysates of tet-on ARPE-19 cells expressing either UL148 or Rh159 fused to an HA tag, i148HA and i159HA, respectively, were collected at the indicated times post doxycycline (dox) induction and analyzed by Western blot for the expression of the indicated proteins and for the abundance of eIF2α phosphorylated at Ser51 (P-eIF2α) using a phospho-specific antibody. (**B**) Pearson's correlation coefficient (*r*) values were calculated using NIH ImageJ software estimate the degree of co-localization between UL148 (HA signal) and the indicated cellular markers. A minimum of 30 cells were analyzed per marker. Arithmetic means for each co-localization analysis result are shown as blue lines, and data points for individual cells analyzed are plotted as circles.

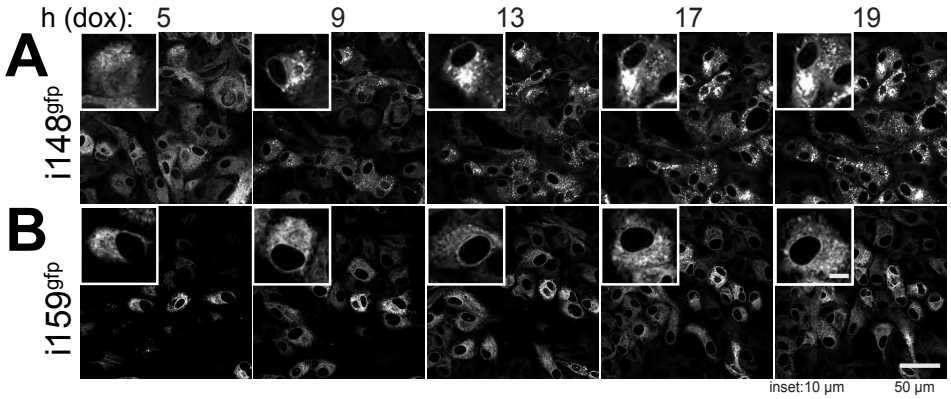

FIG 12. Live Cell Imaging of UL148-GFP and Rh159-GFP during Induced Ectopic Expression. "Tet-on" ARPE-19 epithelial cells that inducibly express either UL148 or Rh159 fused to green florescent protein (gfp), i148^{gfp} (**A**) and i159^{gfp} (**B**), respectively, were induced for transgene expression using 100 ng/mL doxycycline (dox) and imaged using live-cell microscopy. Images from the selected time points (h post treatment with dox, hpt) are shown. Main scale bar represents 50 µm. For inset panels at upper left of each image, which are magnified 2.4× relative to the main image, the scale bar represents 10 µm. Also see SI Movies S2-S3.

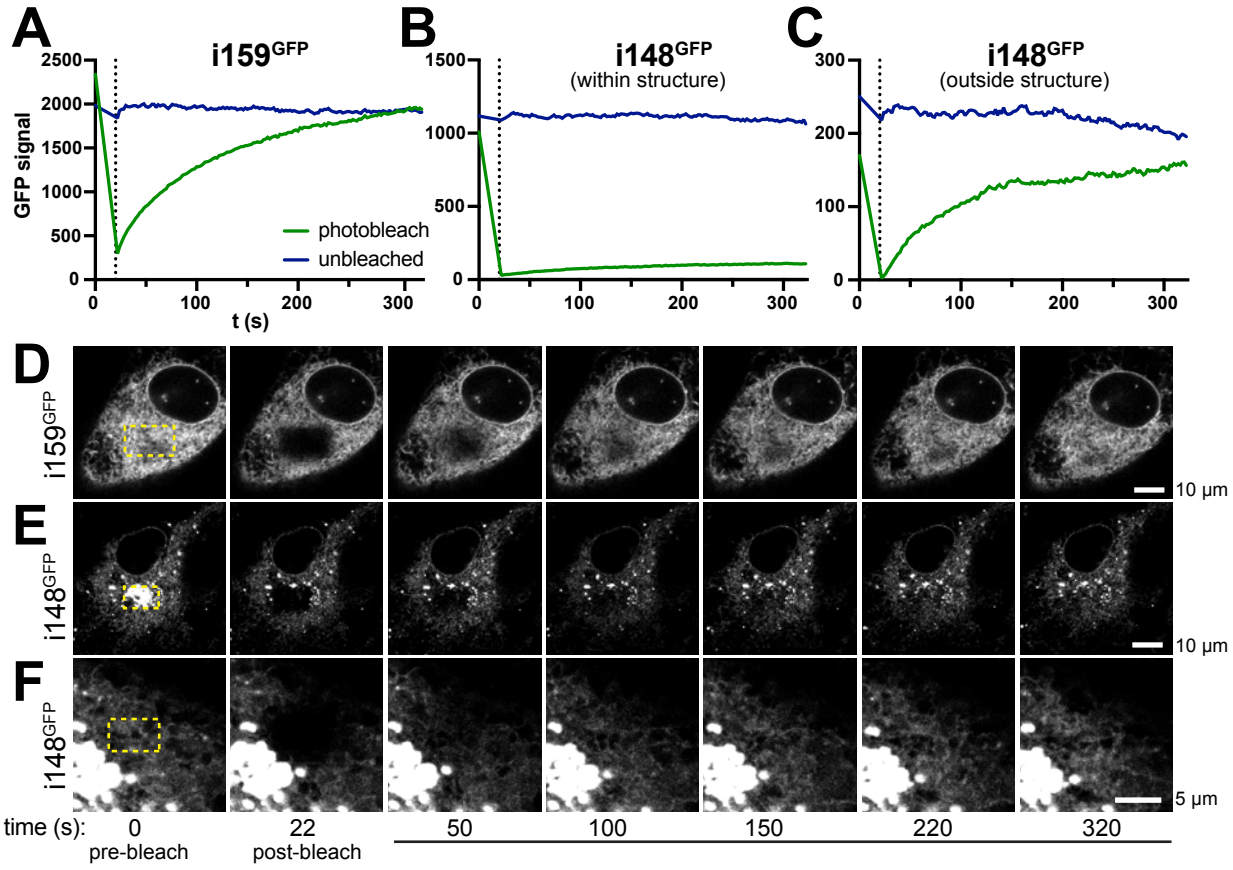

FIG 13. FRAP analysis. ARPE-19 cells that inducibly express Rh159-GFP, i159^{gfp} (**A**) or UL148-GFP, i148^{gfp} (**B-C**) were doxycycline induced for 24 h (100 ng/mL doxycycline (dox). Separate regions of GFP signal in selected cells were photobleached (405 nm laser) or left unbleached, while a third region lacking GFP signal was chosen as a background reference were measured before and during fluorescence recovery after photobleaching (FRAP). Note: background signal was not plotted because values were resolvable from the x-axis. GFP signal intensity is plotted over a time period (seconds, s) starting with an exposure at t=0 (immediately before photobleaching), and including measurements taken every 2 s after photobleaching (0-20 s) until termination of the measurement series at t=322 s (300 s of FRAP). (**D-F**) Images from the selected time points (s, seconds) immediately before and after bleaching, and during fluorescence recovery period. Also see SI Movies S4-S6.

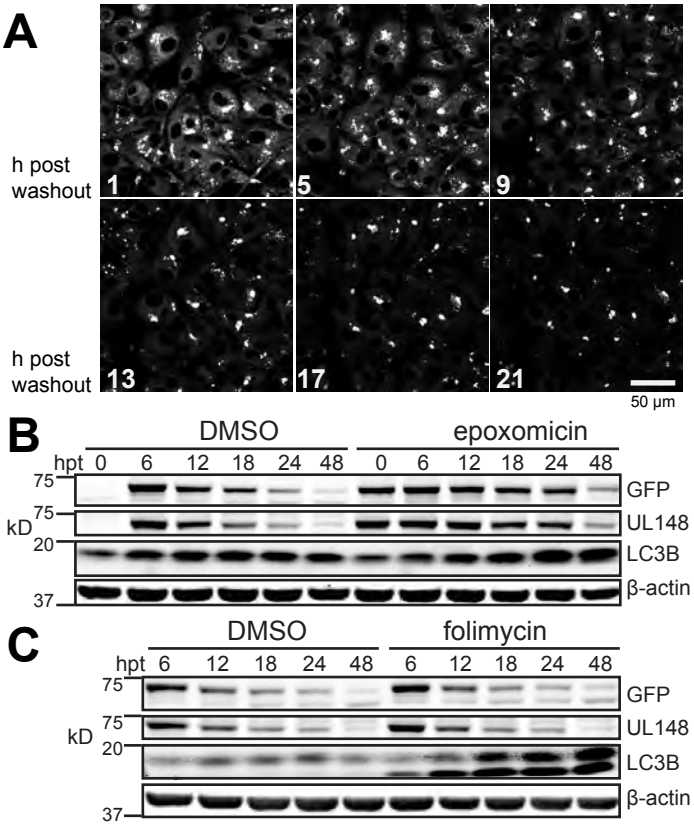

FIG 14: UL148-GFP is stabilized by inhibition of proteasomal but not lysosomal degradation. "Tet-on" ARPE-19 cells that inducibly express UL148-GFP (i148^{gfp}) were induced for 24 h by the addition of 100 ng/mL doxycycline (dox), after which the dox inducing agent was washed out and medium containing either the proteasome inhibitor epoxomicin (20 µM) or the proton pump inhibitor folimycin (115 nM) was added and samples were harvested for Western blot analysis at the indicated times post treatment (h post treatment, hpt) with folimycin or epoximicin. Also see SI Movie S7.

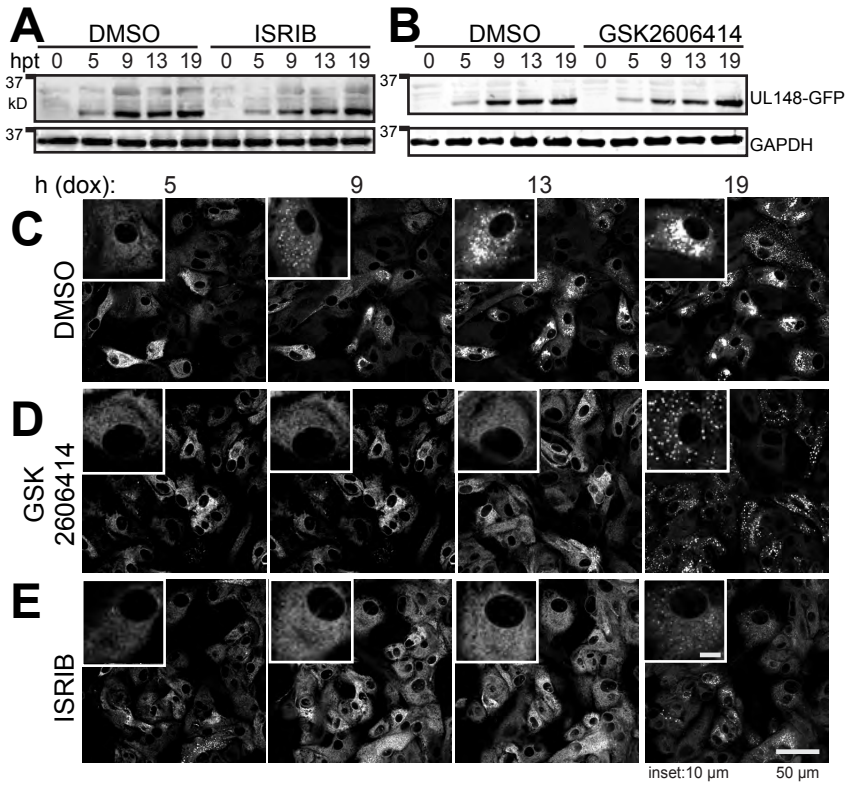

FIG 15. Inhibition of the integrated stress response impedes UL148-mediated ER remodeling. "Tet-on" ARPE-19 epithelial cells that inducibly express either UL148 or Rh159 fused to green florescent protein (gfp), i148^{gfp} (**A**) and i159^{gfp} (**B**), respectively, were induced for transgene expression using 100 ng/mL doxycycline (dox) in the presence of absence of either ISRIB (200 nM) or GSK2606414 (1.1 µM) and monitored by Western blot for expression of UL148-GFP over a series of time points (h post treatment with dox, hpt). (**C-E**): Live-cell imaging of UL148-GFP and Rh159-GFP expression patterns in the presence of ISRIB (200 nM), GSK2606414 (1.1 µM), or DMSO vehicle alone. Main scale bar represents 50 µm. For inset panels at upper left of each image, which are magnified 2.4× relative to the main image, the scale bar represents 10 µm. Also see SI Movies S8-S10.

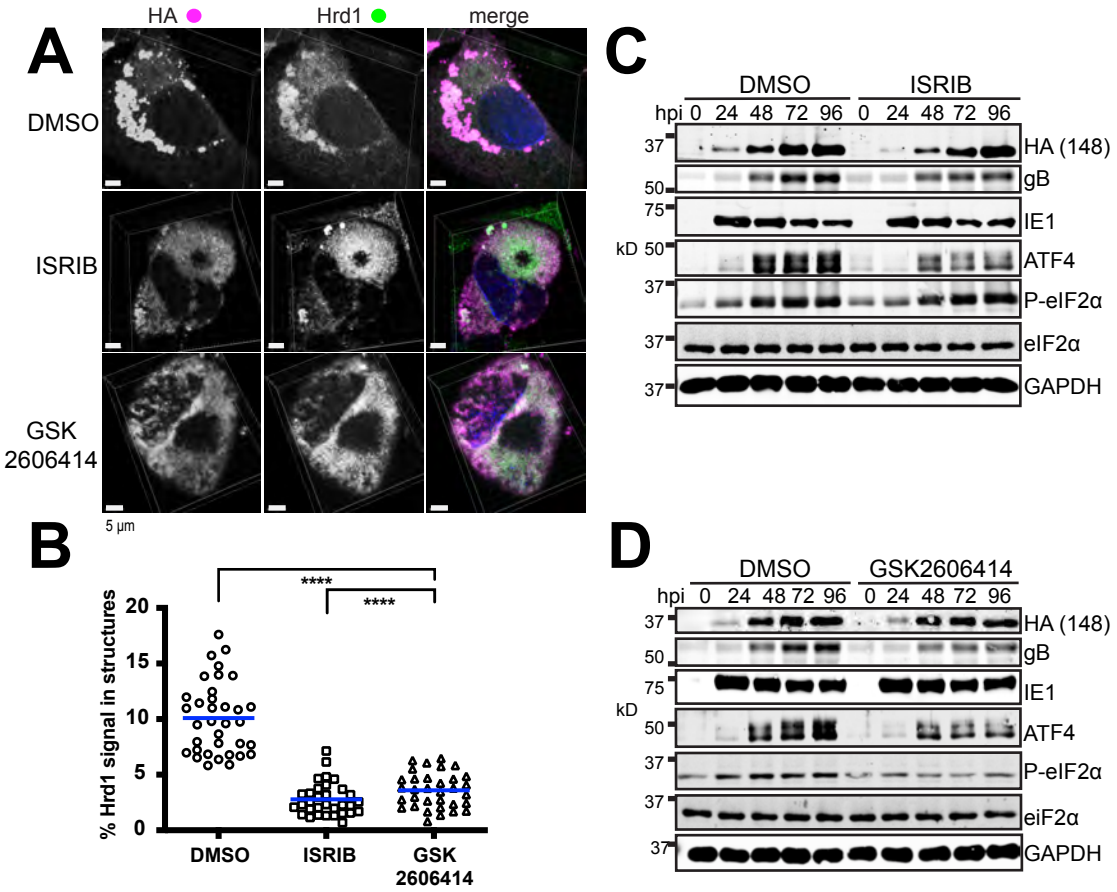

FIG 16. Inhibition of the ISR prevents the coalescence of Hrd1 and UL148 into discrete structures during infection. (A) Representative 3D maximum intensity projections of confocal imaging Z-stacks obtained from cells infected at MOI 1 for 96 h with HCMV strain TB40/E carrying an HA-tagged *UL148*, TB_148^{HA}, and maintained in the presence of ISRIB (200 nM), GSK2606414 (1.1 µM), or DMSO carrier alone (0.1% vol/vol). In merged images HA signal is shown in magenta, Hrd1 in green, and DAPI counterstaining in blue. (B) The percent of Hrd1 antibody signals that were involved in discrete structures at 96 hpi were calculated for a minimum of 30 cells per condition were determined using Imaris x64 9.3.0 software. Statistical significance was determined using a one-way ANOVA followed by Tukey's post-test; **** represents a P-value of <0.0001. The arithmetic mean for each co-localization analysis result is shown as a blue line, and data points for individual cells analyzed are plotted as circles. (C-D) Western blot analyses of fibroblasts infected at MOI 1 with TB_148^{HA} and maintained in the presence of ISRIB (200 nM), GSK2606414 (1.1 µM), or DMSO carrier alone (0.1%); hpi: h post infection (hpi). Note: a phospho-specific antibody was used for detection of eIF2α phosphorylated at Ser51 (P-eIF2α).

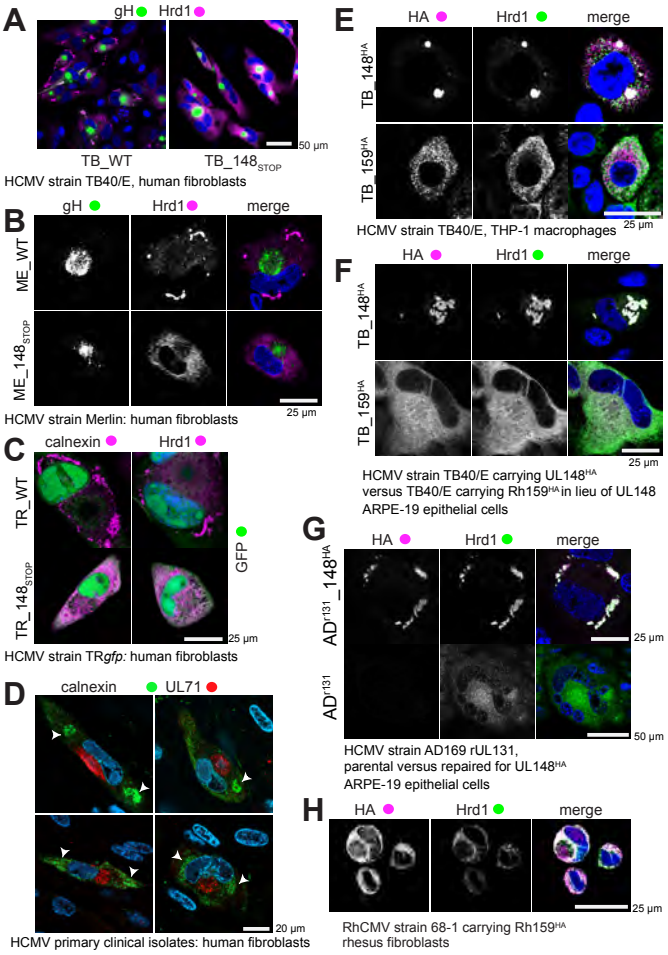

Fig S1: (A) Lower magnification overview of results from Fig 1A-B; confocal indirect immunofluorescence staining of HCMV glycoprotein H (gH) and Hrd1 at 96 h postinfection of human fibroblasts with wildtype HCMV strain TB40/E (WT) versus *UL148*-null derivative TB_148$_{STOP}$. (B) Confocal indirect immunofluorescence staining of gH and Hrd1 at 96 h postinfection of human fibroblasts with wildtype Merlin recovered from BAC-cloned Merlin pAL1393 (ME_WT) or a *UL148*-null derivative of the same virus (ME_148$_{STOP}$.) (C): Confocal indirect immunofluorescence staining of gH and Hrd1 at 96 h postinfection of human fibroblasts with wildtype HCMV strain TRgfp recovered from BAC-cloned TRgfp (TR_WT) or a *UL148*-null derivative of the same virus (TR_148$_{STOP}$). (D) Confocal indirect immunofluorescence staining of the viral tegument protein UL71 and calnexin at 5 days postinfection of human fibroblasts with primary clinical HCMV isolates obtained from patient throat swabs. (E) Confocal indirect immunofluorescence staining against HA and Hrd1 in THP-1 macrophages fixed at 96 h postinfection with HCMV strain TB40/E derivative viruses TB_148^{HA} or TB_159^{HA}; note: THP-1 monocytes were differentiated using phorbol ester treatment. (**F**) Confocal indirect immunofluorescence staining of HA and Hrd1 in ARPE-19 epithelial cells infected for 96 h with either TB_148^{HA} or TB_159^{HA}. (**G**) Confocal indirect immunofluorescence staining of HA and Hrd1 in ARPE-19 epithelial cells infected for 96 h with HCMV strain AD169 repaired for *UL131* and to which an HA-tagged UL148 CDS from TB40/E was restored to the native *UL148* locus (AD^{r131}_148^{HA}) or with a parental AD169 virus repaired for *UL131* to which *UL148* was not restored (AD^{r131}). Notes: (i) a functional *UL131* is required for efficient infection of epithelial cells; (ii) the difference in scale bar between ADr131 and ADr131_148^{HA} is because with ADr131 we did not have a viral marker (e.g., HA) to identify infected cells, so the appearance of syncytia and the characteristic kidney-bean shaped nucleus was used to indicate infected cells, hence the use of a slightly lower magnification. (**H**) Confocal indirect immunofluorescence staining of telomerase-immortalized rhesus fibroblasts infected with BAC derived rhesus CMV (RhCMV) strain 68-1 carrying an HA-tag at the C-terminus of Rh159.

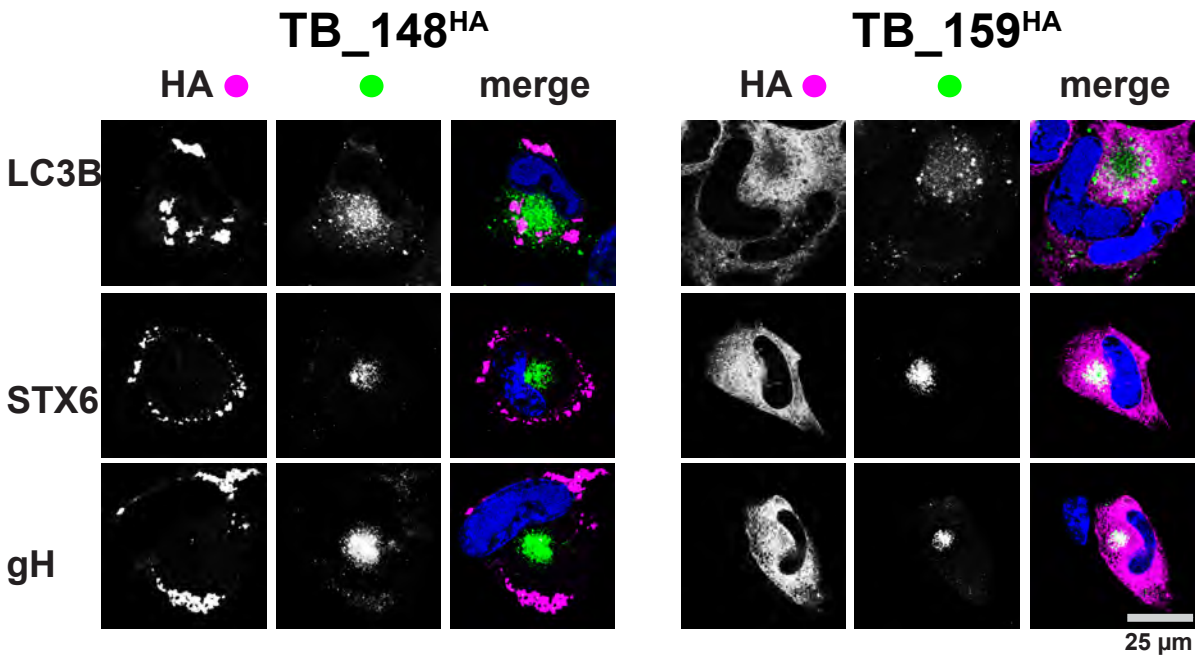

FIG S2: Confocal microscopy of LC3B, syntaxin-6 and glycoprotein H staining during HCMV infection. Human fibroblasts were infected with the indicated viruses for 96 h and then fixed, permeabilized, and stained using antibodies specific for the indicated proteins. Indirect immunofluorescence images were captured using a 63X objective on a Leica SP5 confocal microscope. gH: glycoprotein H, STX6: syntaxin-6.

TABLE S1. Oligonucleotide primers and synthetic DNAs used in this study

Name	Sequence (5' to 3')
148_eGFP_Fw	ACCTGGTGTCGCGGCGTCGGATGGTGAGCAAGGGGGAGGAGCTTTTTACTGGCGTTGTTC
Gibs_eGFP_Rv	CGGCCGCCACTGTGCTGGATTACTTATACAGCTCGTCCATACCCAG
Gib_148_Fw	TGTGGTGGAATTCTGCAGATTGCCACCATGTTGCGCTTGCTG
148_noStopRv	CCGACGCCGCGACACCAGGTAGGTTATC
159_eGFP_Fw	TCTAAAACGCAGTCGTGAAGCTCATATGGTGAGCAAGGGGGAGGA
159_noStop_Rv	ATGAGCTTCACGACTGCGTTTTAGAAGTG
Gibs_159_Fw	TGTGGTGGAATTCTGCAGATTGCCACCATGGCCTACAACAGC
Rh159_Fw	TGTGGTGGAATTCTGCAGATACCATGGCCTACAACAGCTTCCTTCTCAGCTGCCTTACCATCGCAC TTTTACTG
Rh159_HA_Rv	CGGCCGCCACTGTGCTGGATCTATTAGGCGTAGTCTGGGACGTCGTATGGGTAATGAGCTTCACG ACTGCGTTTTAGAAGTG
PpuISceKanGibs_Fw	CATTCACCTGAACCCATAGGTCCTGCCTGGCAGAGAATCTTAGGGATAACAGGGTAATCG
PpuISceKanGibs _Rv	AGATTCTCTGCCAGGCAGGACCTATGGGTTCAGGTGAATGGCCAGTGTTACAACCAATTA
Rh159_Fw_recomb	GGGCGGTGGCCGGCACGCCGCATTTCCTAACCCGCGCAGCATGGCCTACAACAGCTTCCT
Rh159_Rv_recomb	CGCGAACGACGTGTGACGAGGACGTGGTTTCCGCAAGCCTTTAGGCGTAGTCTGGGACG
TB_Rh159HA_seq_Fw	AGTGTTTATGAGTCGGGCGG
REV TB_Rh159HA_seq	GTGGCGACGTGGATTTCTTG
EGFP-P2A-3XHA	GTCGACTGGATCCGGTACCGAATTCGCCACCATGGTGAGCAAGGGGGAGGAGCTTTTTACTGGC GTTGTTCCCATCCTGGTTGAGTTGGATGGGGATGTCAACGGCCACAAGTTCAGCGTTTCTGGAGA AGGAGAAGGCGACGCAACCTATGGGAAGCTCACTTTGAAATTCATATGCACCACCGGTAAACTCC CAGTCCCCTGGCCTACCCTGGTCACTACCTTGACATATGGAGTTCAGTGCTTTTCTCGATACCCCG ACCACATGAAGCAGCACGATTTTTTCAAATCTGCAATGCCCGAGGGCTATGTACAAGAGAGGACCA TTTTCTTCAAAGACGACGGCAATTACAAGACCAGGGCCGAGGTCAAATTTGAAGGGGACACTCTTG TGAATCGGATCGAACTTAAAGGGATCGATTTCAAAGAGGACGGAAACATACTGGGGCATAAGCTG GAATACAACTACAATAGCCATAATGTTTACATTATGGCAGACAAGCAGAAAAACGGTATTAAGGTCA ACTTCAAGATACGGCATAACATTGAAGATGGGTCAGTCCAGCTTGCTGACCATTATCAGCAGAATA CACCCATTGGCGATGGTCCCGTGCTTTTGCCTGACAACCACTACCTTTCTACCCAAAGCGCATTGT CAAAAGATCCTAACGAGAAGAGAGATCATATGGTCCTTTTGGAGTTCGTAACCGCAGCTGGTATAA CTCTGGGTATGGACGAGCTGTATAAGGGCTCAGGGGCTACAAATTTTAGTCTCCTTAAACAAGCCG GAGATGTCGAAGAGAACCCTGGGCCTTACCCATATGACGTTCCTGACTATGCCGGTTACCCCTAT GATGTGCCAGATTATGCCGGATCTTATCCTTACGATGTACCTGACTATGCAGGTGGGAGTGGCAT GAATTACGTGGGGCAGC
Gibs_Age_159_Fw	CCGTACCACTTCCTACCCTCGTAAACCGGTGCCACCATGGCCTACAACAG
Gibs_Mlu_GFP_Rv	ACCCGGCGCGGAGGCCAGATCTTAACGCGTTTACTTATACAGCTCGTCCATACC
tRFP linker Fw	CCACTTCCTACCCTCGTAAACCGGTGAATTCGCCACCATGAGCGAGCTGAT
tRFP linker Rv	GCGCGGAGGCCAGATCTTAACGCGTGCGGCCGCTCGAGAATTCATCTGTGCCCCAGTTTGC

TABLE S2. Antibodies Used in Immunofluorescence Microscopy

Primary Antibody	Host species	Isotype	Clone	Vendor	Catalog No.	Dilution used
Calnexin	Mouse	mAb IgG1	37	BD Biosciences	610523	1:50
Calnexin	Rabbit	mAb IgG	C5C9	Cell Signaling Tech.	2679	1:50
Syntaxin 6	Rabbit	mAb IgG	C34B2	Cell Signaling Tech.	2869	1:50
SYVN1 (Hrd1)	Rabbit	mAb IgG	D3O2A	Cell Signaling Tech.	14773	1:500
SEL1L	Rabbit	pAb	n/a	Sigma	S3699	1:50
KDEL	Mouse	IgG2a	10C3	Enzo Life Sci., Inc.	ADI-SPA-827-D	1:50
PDI	Rabbit	mAb IgG	C81H6	Cell Signaling Tech.	3501	1:50
Herp (HerpUD1)	Rabbit	pAb IgG	n/a	Proteintech	10813-1-AP	1:50
VCP	Mouse	IgG2a	5	Invitrogen / Life Technologies	MA3-004	1:50
Calreticulin	Rabbit	mAb IgG	D3E6	Cell Signaling Tech.	12238	1:200
Ribophorin 1 (RPN1)	Rabbit	pAb IgG		ThermoFisher / Invitrogen	PA5-65662	1:50
EDEM-1	Mouse	mAb IgM	D-1	Santa Cruz	sc-377394	1;50
GABARAP	Rabbit	mAb	E1J4E	Cell Signaling Tech.	13733	1:200
LC3B	Rabbit	mAb	D11	Cell Signaling Tech.	3868	1:200
HA epitope	Chicken	IgY		Bethyl	A190-106A	1:200
HCMV glycoprotein H (gH)	Mouse	IgG2b	14-4b	Gift of William J. Britt, M.D.	n/a	1: 50
Reticulon-3 (RTN3)	Mouse	IgG2a		ThermoFisher / Invitrogen	MA5-15538	1: 200
HA epitope	Rabbit	pAb		Bethyl	A190-108A	1:1000
Secondary Antibody	**Host species**	**Isotype**		**Vendor**	**Catalog No.**	**Dilution used**
Alexa Fluor 488 anti-Mouse IgG (H+L), cross adsorbed	Goat	IgG		ThermoFisher / Invitrogen	A11001	1:1000
Alexa Fluor 488 anti-Rabbit IgG (H+L) Cross-Adsorbed	Goat	IgG		ThermoFisher / Invitrogen	A11008	1:1000
Alexa Fluor 594 anti-Rabbit IgG (H+L) Cross-Adsorbed	Goat	IgG		ThermoFisher / Invitrogen	A11012	1:1000
Alexa Fluor 594 anti-Mouse IgG (H+L) Cross-Adsorbed	Goat	IgG		ThermoFisher / Invitrogen	A11005	1:1000
Alexa Fluor 647 anti-Chicken IgY (H+L)	Goat	IgG		ThermoFisher / Invitrogen	A11039	1:1000